MODIFICATION OF SINGLE WALLED CARBON NANOTUBE THIN FILMS
FOR SUPERCAPACITOR ELECTRODES

A THESIS SUBMITTED TO

THE GRADUATE SCHOOL OF NATURAL AND APPLIED SCIENCES

OF

MIDDLE EAST TECHNICAL UNIVERSITY

BY

METE BATUHAN DURUKAN

IN PARTIAL FULFILLMENT OF THE REQUIREMENTS

FOR

THE DEGREE OF MASTER OF SCIENCE

IN

METALLURGICAL AND MATERIALS ENGINEERING DEPARTMENT

SEPTEMBER 2017

Approval of the thesis

MODIFICATION OF SINGLE WALLED CARBON NANOTUBE THIN FILMS FOR SUPERCAPACITOR ELECTRODES

Submitted by **METE BATUHAN DURUKAN** in partial fulfillment of the requirements for the degree of **Master of Science in Metallurgical and Materials Engineering Department, Middle East Technical University** by,

Prof. Dr. Gülbin Dural Ünver
Dean, Graduate School of **Natural and Applied Sciences, METU**

Prof. Dr. Hakan Gür
Head of Department, **Metallurgical and Materials Eng. Dept., METU**

Assoc. Prof. Dr. Hüsnü Emrah Ünalan
Supervisor, **Metallurgical and Materials Eng. Dept., METU**

Examining Committee Members:

Prof. Dr. Tayfur Öztürk
Metallurgical and Materials Engineering Dept., METU

Assoc. Prof. Dr. Hüsnü Emrah Ünalan
Metallurgical and Materials Engineering Dept., METU

Prof. Dr. Zeki Aktaş
Chemical Engineering Dept., Ankara University

Prof. Dr. Kadri Aydınol
Metallurgical and Materials Engineering Dept., METU

Assist. Prof. Dr. Simge Çınar
Metallurgical and Materials Engineering Dept., METU

Date: 06.09.2017

iii

I hereby declare that all information in this document has been obtained and presented in accordance with academic rules and ethical conduct. I also declare that, as required by these rules and conduct, I have fully cited and referenced all material and results that are not original to this work.

Name, Last name: Mete Batuhan Durukan

Signature   :

ABSTRACT

MODIFICATION OF SINGLE WALLED CARBON NANOTUBE THIN FILMS FOR SUPERCAPACITOR ELECTRODES

Durukan, Mete Batuhan

MSc., Metallurgical and Materials Engineering Department

Supervisor: Assoc. Prof. Dr. Hüsnü Emrah Ünalan

September 2017, 94 pages

Electrochemical capacitors, or supercapacitors, attracted a lot of attention in recent years due to their stability under numerous charge-discharge cycles, high charge discharge rates, and high power density when compared to batteries and conventional capacitors. Since their energy density is much lower than batteries, current research on supercapacitors is focused on improving the energy density through the development of novel active materials and innovative design of the electrodes.

Carbon nanotubes are promising materials for batteries and supercapacitors with their unique morphology and electrical properties. They have highly accessible surface area, efficient electronic transport without scattering and high stability, all of which makes them suitable candidates as electrode materials for electrochemical capacitors. Furthermore, their composites in conjunction with pseudocapacitive materials are also investigated extensively primarily for the electrochemical performance enhancement.

In this work, single walled carbon nanotube (SWNT) thin films are used as supercapacitor electrodes. Main idea of this thesis is to fabricate nanocomposite supercapacitors and micro-supercapacitors using cost effective and simple and scalable routes. In this regard, in the first part, SWNT thin film electrodes are used as current collectors and decorated with cobalt oxide (Co_3O_4) nanoflakes using electrodeposition and consecutive annealing process. A gravimetric capacitance of 313.9 $F.g^{-1}$, corresponding to an areal specific capacitance of 70.5 $mF.cm^{-2}$ is obtained from the fabricated electrodes at a scan rate of 1 mV/s. A capacity retention of up to 80% following 3000 charge/discharge cycles is obtained for the fabricated nanocomposite electrodes, while morphological evolution of the electrodes was monitored through high-resolution transmission electron microscopy during cycling. In the second part, are laser patterned SWNT thin films on glass substrates are used for the fabrication of micro-supercapacitors. Laser patterning is proposed for the formation of interdigitated electrodes. A specific capacitance of 3.50 $mF.cm^{-2}$ at a scan rate of 10 mV/s was obtained from the SWNT buckypaper that was laser ablated to form interdigitated finger electrodes. A capacity retention up to 97% was attained at an applied current of 3 mA following 1000 charge/discharge cycles.

Keyword: carbon nanotubes, energy storage, supercapacitors, cobalt oxide, micro-supercapacitors

ÖZ

SÜPERKAPASİTÖR ELEKTRODLARI İÇİN TEK DUVARLI KARBON NANOTÜP İNCE FİLMLERİNİN MODİFİKASYONU

Durukan, Mete Batuhan
Yüksek Lisans, Metalurji ve Malzeme Mühendisliği Bölümü
Tez Yöneticisi: Doç. Dr. Hüsnü Emrah Ünalan

Eylül 2017, 94 Sayfa

Elektrokimyasal kapasitörler, ve ya süperkapasitörler, çok sayıda şarj-deşarj altındaki stabiliteleri, hızlı şarj-deşarj kapasiteleri ve yüksek güç yoğunlukları nedeni ile son yıllarda piller ve konvansiyonel kapasitörlere göre oldukça ilgi çekmişlerdir. Enerji yoğunlukları pillerden çok daha düşük olduğu için süregelen araştırmalar enerji yoğunluğunun arttırılması için yeni geliştirilen aktif malzemeler ve inovatif elektrot dizaynına geliştirilmesine yoğunlaşmıştır.

Karbon nanotüpler özgün morfolojileri ve elektriksel özellikleri sayesinde hem bataryalar hem de süperkapasitörler için gelecek vaat eden malzemelerdir. Yüksek erişilebilir yüzey alanı, saçılıma uğramayan verimli elektron transferi ve yüksek stabilitesi KNT'lerin elektrokimyasal kapasitör uygulamaları için oldukça uygun adaylar olarak kılmaktadır. Üstelik, psödokapasitif malzemeler ile birlikte nanokompozit haline getirilen KNT'ler gelişmiş elektrokimyasal performans nedeniyle derinlemesine araştırılmaktadır.

Bu çalışmada, tek duvarlı karbon nanotüp bazlı süperkapasitör ince filmler süperkapasitör elektrotları olarak kullanılmışlardır. Bu tezin asıl amacı uygun maliyetli ve seri üretim için ölçeklendirilebilecek basit bir yol ile nanokompozit süperkapasitörlerin ve mikro-süperkapasitörlerin üretilmesidir. Bu bağlamda, ilk parçada, KNT ince filmleri akım toplayıcı olarak kullanılmış ve elektrokaplama ve ardından gelen tavlama prosesi sayesinde kobalt oksit (Co_3O_4) nanopulları ile dekore edilmiştir. Üretilen elektrotların 1 mV/s tarama hızında gravimetrik kapasitansı 313.9 $F.g^{-1}$ ve buna eş değerde alansal kapasitansı 70.5 $mF.cm^{-2}$ olarak elde edilmiştir. 3000 döngüde, üretilen elektrotların korunan kapasitansı %80'e kadar vararken aynı zamanda yüksek çözünürlüklü geçirimli elektron mikroskopu kullanılarak morfolojik değişimler gözlemlenmiştir. İkinci kısımda ise cam üzerinde lazer ile desenlendirilmiş tek duvarlı KNT ince filmleri mikro-süperkapasitör üretmek için kullanılmıştır. Birbirine geçmiş yapıda elektrotların üretimi için lazer ile desenlendirme önerilmiştir. Lazer ablasyonu ile elde edilen birbirine geçmiş parmak elektrotların spesifik kapasitansı 10 mV/s tarama hızında 3.50 $mF.cm^{-2}$ olarak bulunmuştur. 3 mA akımda uygulanan 1000 döngü doldurma-boşaltma sonucunda korunan kapasitans oranı %97 olarak elde edilmiştir

Anahtar Kelimeler: karbon nanotüp, enerji depolama, süperkapasitör, kobalt oksit, mikro-süperkapasitör

"Pliancy and weakness are expressions of the freshness of being.
Because what has hardened will never win.'

Andrei Tarkovsky, Stalker (1979)

To my family and my dearest friends,

ACKNOWLEDGEMENTS

Firstly, I would like to express my deepest gratitude to my advisor Assoc. Prof. Dr. H. Emrah Ünalan, for his support, guidance and patience throughout the study. It is a great honor to work under his supervision.

I owe my deepest gratitude to my labmates colleagues and dearest friends, Şahin Coşkun, Doğa Doğanay, Selin Özkul, Recep Yüksel, Sevim Polat, Doğancan Tigan, Alptekin Aydınlı, Ece Alpugan, Itır Bakış Doğru, Onur Türel, İpek Bayraktar, Serkan Koylan, and Şeyma Koç.

I also appreciate the great moral support from my colleagues and my dearest friends Ziya Çağrı Torunoğlu, Mustafacan Kutsal and Mehmet Hazar Şeren who helped me throughout this study. They all will be remembered for their intimate friendship. I also would like to thank Bengisu Yaşar, Ayşe Merve Genç Ünalan and Serkan Yılmaz for their help and support.

I am also thankful to Merve for her support through my constant grumbling and encouragement in my hardest times. I will always remember her patience and the love she has given.

And finally, I would like to thank my family who always gave me hope during my studies. Thank you for everything, thank you for always being there for me.

TABLE OF CONTENTS

LIST OF TABLES

LIST OF FIGURES

CHAPTER 1

INTRODUCTION

1.1   Introduction to Electrochemical Capacitors and their Current Status

Early examples of capacitors date back before the invention of batteries in 1800, *Volta's pile*, in which 18th century researchers relied on *Leyden jar* for energy storage. Leyden jar consisted of a silver foil (as the electrodes) coated both inside and outside of a glass jar, which acted as a dielectric material. Inner silver foil could be charged with an electrostatic generator, which was allowed by the outer foil being grounded and could provide an electrical discharge for simple devices back then [1,2]

First patented in 1957, electrochemical capacitors (ECs), also known as supercapacitors (SCs), have been known for almost 60 years [3]. SCs are based on a capacitor making use of the high surface area of carbon [3,4]. ECs are attracted much more attention as potential energy storage devices due to their fast discharge rate, long cycle life and high power density [5]. Benefiting from these properties, ECs are highly appealing when slow power uptake and delivery of Li-ion batteries are considered [6].

With modern advances in technology, there are several utilization areas in which the SCs replaced batteries to complement the need for the increasing power demands of energy storage systems. One such commercialization example came from Maxwell Technologies. Their supercapacitors were used in start-stop systems, assisting the power demand, and short-term backup for powering the sensors of automobiles (used by General Motors, Lamborghini, Continental AG and PSA) [7]. Moreover, Maxwell Technologies' supercapacitor modules (Fig. 1.1) were used in energy grid systems, which stores excess energy obtained from the solar and wind power systems and excess energy stored is deployed when the demand is high [8]. Another example is the doors of Airbus A380. Supercapacitors are used to provide high power output, allowing the aircraft's heavy doors to operate independently in a case of emergency [9].

Figure 1.1 Ultracapacitor modules with different specifications from Maxwell Technologies [10].

There are also buses that operates only with SCs. In 2009, a Chinese company in conjuction with Volvo, used SCs to power up inner city buses in Shangai (Figure 1.2). These supercapacitors were made of activated carbon, which had only 5% of the energy density of the lithium ion batteries. While it needs to be charged in every 3 to 5 miles, it was reported that the lifetime fuel savings can achieve at least $200,000 [11].

Figure 1.2 A photo of an electric bus that operate only with supercapacitors in Shangai, China [11].

1.2   Working Principles of ECs

Both batteries and SCs depend on electrochemical processes for storing energy. The difference between these two devices come from their relative energy and power densities. Li-ion batteries depend on the intercalation of Li^+ ions into the bulk of the electrode, which allows redox reactions to occur in a diffusion-controlled manner, showing slow charge/discharge rates. On the other hand, energy storage in SCs are confined to the surface of the electrodes. Thus, these devices have much faster reaction rates compared to batteries, yet also have much less energy density [12].

Conventional capacitors and SCs rely on the same working principles. Their classification is done considering their physical states or the dielectric mechanism. Classification of capacitors can be seen in the chart provided in Figure 1.3. Unlike batteries, conventional capacitors can also rapidly store and release energy like SCs. However, what differs is that SCs utilize high surface area electrodes and much
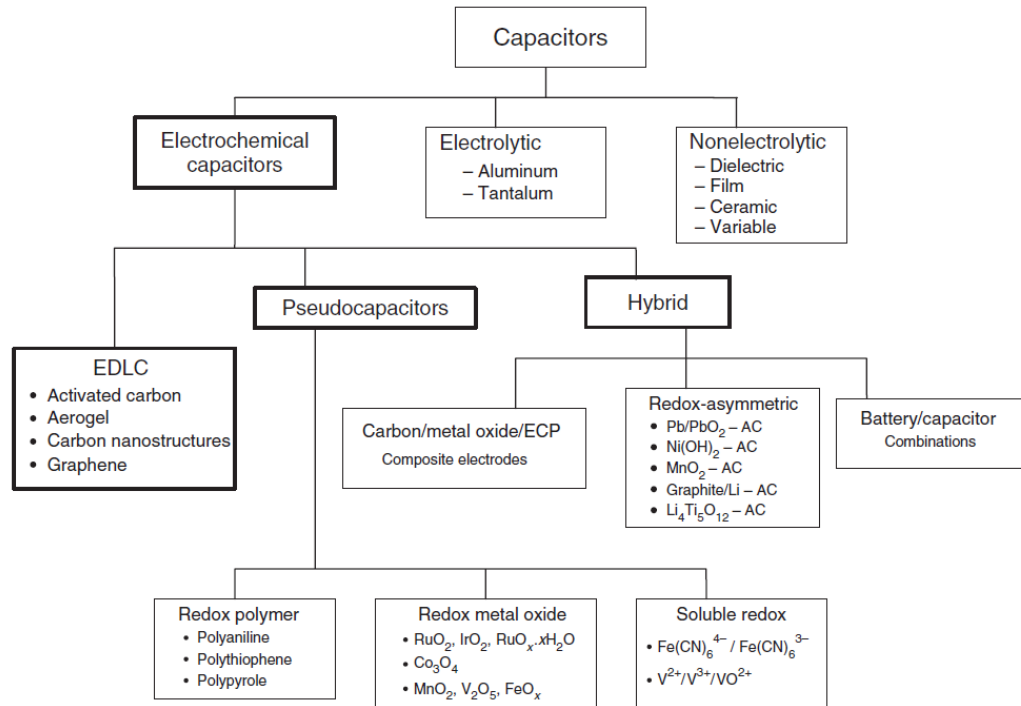
Figure 1.3 General classification of capacitors with respect to their physical states or their dielectric material [1]

thinner dielectrics than conventional capacitors. This allows SCs to possess both higher capacitance and energy density up to 10,000 times that of a conventional capacitors [1]. Having more capacitance than conventional capacitors and very rapid energy storage and release unlike batteries' slow reaction rates, SCs' have an exclusive position between those two. This can be observed with respect to the energy and power densities in Ragone Plot (Figure 1.4).
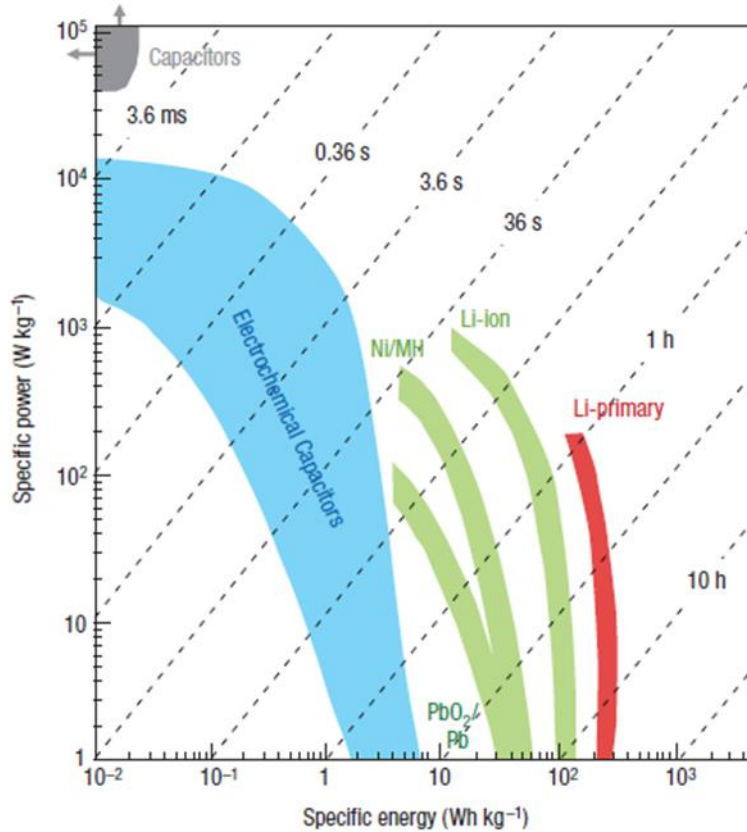
Figure 1.4 Ragone plot comparing SCs to other energy storage systems [6].

Conventional nonelectrolytic capacitors consist of two parallel plate electrodes and a dielectric material between them (Figure 1.5). Charge is stored electrostatically when a potential difference is applied; causing migration of the positive and negative charges towards the surface of the electrodes of opposite polarity. Capacitance of a capacitor is measured in farads (F) using the equation below:

$$C = \frac{Q}{V}$$

4

,where Q is the electric charge on the electrodes and V is the potential difference between them. In a parallel plate capacitor, capacitance can also be calculated using,

$$C = \frac{\varepsilon_0 \varepsilon_r A}{D}$$

,where ε_0 and ε_r are permittivity of free space and dielectric constant, respectively. A is the area of the electrodes and D is the distance between the electrodes [1].
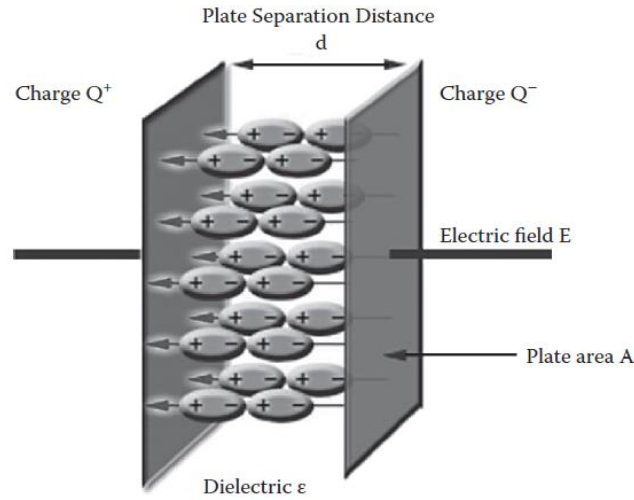
Figure 1.5 Schematic representation of a conventional capacitor device [2].

A typical supercapacitor device consist of two electrodes separated either by a separator wetted with an electrolyte or a solid electrolyte. Solid electrolyte acts both as a separator and charge carrier. Charge mechanism differs in SCs depending on the electrode active materials and they are classified as electrochemical double layer capacitors (EDCLs) and pseudocapacitors (or redox capacitors), which will be discussed later. They commonly use high surface area electrode materials, which is primarily active carbon for EDLC's and metal-oxides for pseudocapacitors. In order to make use of the whole surface of electrode materials, ion size of the electrolyte should be coherent with the pore size of the prepared electrodes. If the pore size of the prepared electrode is smaller than the ion size of the electrolyte, ion adsorption cannot be fully achieved. This drastically decreases the capacitance of the system. Thus, surface area of the material and pore size of the electrode for both EDLCs and pseudocapacitors should be carefully engineered and appropriate electrolytes should be selected to obtain

the highest capacitance. It is also possible to use partial desolvation of ions for the adsorption of ions through pores that are smaller than 2 nm to increase specific capacitance [13].

Characteristic properties/performance/parameters for typical capacitors, batteries and supercapacitors are tabulated and provided in Table 1.1.

Table 1.1 Characteristic properties/performance/parameters for capacitors, batteries and supercapacitors [1].

Characteristics	Capacitor	Battery	Supercapacitor
Storage Mechanism	Electrostatic	Chemical	Electrostatic for EDCLs Redox reactions for pseudocapacitors
Charge Storage	Charged plates	Entire electrode	Electrode/electrolyte interface
Energy Density (Wh/kg)	<0.1	20-150	1-10
Power Density (W/kg)	>10 000	<1000	500-10 000
Discharge Time (s)	$10^{-6} - 10^{-3}$	0.3 h – 3 h	Seconds to minutes
Cycle Life	$>10^6$	$>10^6$	~1500

1.2.1 Electrical Double Layer Capacitance (EDLC)

Energy storage in EDLCs are purely dependent on electrostatic charge accumulation at the surface of the materials, which are typically carbons and their derivatives. Charge is stored at the electrode/electrolyte interface, making the surface area of the material and permeability of the electrolyte ions through pores as the main parameters for capacitance [14]. Carbon materials being very abundant and highly conductive makes them significant for such energy storage devices.

First model of electrical double layer was suggested by von Helmholtz [15] using a quasi-2-dimensional system having oppositely charged layers separated by a small atomic distance. While the original model was first adopted for colloid interfaces, it was later adapted to the case of electrode interfaces and latter model was further modified realizing that the ions could be subjected to thermal fluctuation and would not remain static at the solution side of the double layer [16]. The model which is called "diffuse" double-layer capacitance introduced by Gouy was again not completely true since the ions were assumed to be point charges. This lead to an incorrect potential profile at the electrode surface and excessively large potential difference prediction was defined as the rate of change of net ionic charge on the solution side and change of metal solution across the interphase. Chapman [17] mathematically combined diffuse layer model with Boltzmann's energy distribution equation and Poisson's equation to enlarge upon the relation of the distance from the electrode surface with ionic space charge density in the interphasial region to the second derivative of electric potential. It should be noted that the mathematical derivation from the combination of Boltzmann's energy distribution function and Poissons's equation is referred as Poisson-Boltzmann equation. Later on, Stern [18] overcame the Gouy-Chapman's overestimation of the double layer capacitance by taking into account of Langmuir's adsorption isotherm for inner region of the ion distribution. Moreover, region beyond the adsorption layer was treated in terms of a diffuse region of distributed ionic charge. Geometric limit of the adsorption region of ions could also be calculated easily if the ions were acknowledged as having finite size. With this model, Stern calculated the overall capacitance by two components; Helmholtz type of double layer having a capacitance C_H, and a diffuse region of double layer having a capacitance C_{diff}. Thus, overall double layer capacitance, C_{dl}, was calculated as a series relation according to an equivalent circuit [5];

$$\frac{1}{C_{dl}} = \frac{1}{C_H} + \frac{1}{C_{diff}}$$

It should be noted that the overall double layer capacitance is governed by the smaller component of C_H or C_{diff} [5]. Schematics of Helmholtz, Gouy-Chapman and Stern type of double layer models can be seen in the following figure, Figure 1.6.
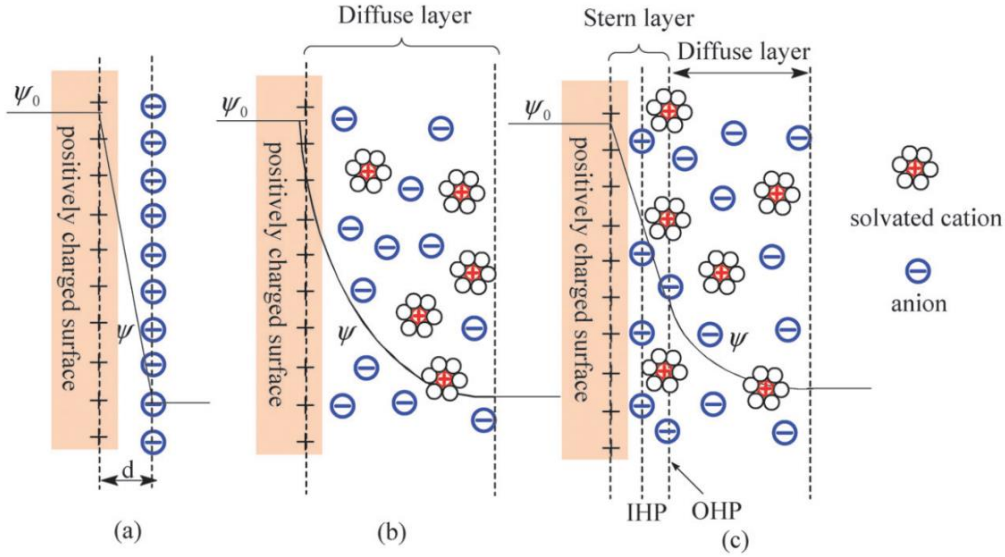
Figure 1.6 Electrical double layer models: (a) Helmholtz model, (b) Gouy-Chapman model, and (c) Stern model. IHP and OHP refers to the inner Helmholtz plane and outer Helmholtz plane, respectively. ψ_0 and ψ refers to the potentials at the electrode surface and the electrode/electrolyte interface, respectively [14].

As mentioned before, carbon derivatives are the main active materials of commercialized supercapacitors that utilizes EDLC for energy storage. Carbon derivatives in commercialized supercapacitors are generally in the form of activated carbon [19], yet other forms and morphologies of carbons have been researched extensively such as graphenes [20,21], carbon fibers [22–24], nanotubes [25,26], nano-onions [27,28], aerogels [29,30] and glassy carbons [31]. Typical properties and capacitance values of carbons can be seen in Table 1.2. These specific carbon materials have attracted a lot of attention due to their high conductivity, controllable specific surface area and pore structure, good corrosion resistance, high temperature stability and processability [19].

Table 1.2 Different carbon materials and their corresponding specific surface areas and capacitance values.

Carbon Materials	Specific surface area $(m^2.g^{-1})$	Aqueous Electrolyte $(F.g^{-1})$
Activated carbons	1000-3500	<200
Functionalized porous carbons	1000-2000	170-220
Carbon nanotubes	120-500	50-100
Carbon cloth	2500	100-200
Carbon aerogel	400-1000	100-125

1.2.2 Pseudocapacitance

As discussed before, double-layer capacitance is relatively low since the charge is only stored physically on the surface of the carbonaceous materials and manipulation of ion accessibility and porosity is limited [2]. Instead of EDLC type of materials, pseudocapacitive materials can store much more charge through electrochemical reduction-oxidation reactions, also known as redox or faradaic reactions. In fact, the term "pseudo" has a meaning of being almost, approaching or trying to be in Greek. Thus, pseudocapacitor means an electrode having similar electrochemical behavior to EDLC but with different energy storage mechanism [32].

Pseudocapacitive materials store energy with fast, reversible redox reactions at the surface of the active materials, such as transition metal oxides or conducting polymers. Reactions start with mass transfer of reactant towards the electrode interface to have electron transfer at the electrode/electrolyte interface. Afterwards, preceding chemical reactions take place via adsorption or desorption mechanisms at the surface of the electrode. Ruthenium oxide (RuO_2) [33], iron oxide (Fe_3O_4) [34], zinc oxide (ZnO) [35], manganese oxide (MnO_2) [36,37], cobalt oxide (Co_3O_4) [38,39] and nickel oxide (NiO) [40] are a few examples of such metal oxides; while polyaniline, polypyrrole and polythiophene are examples of conductive polymers utilized in SCs [41].

RuO$_2$ was the first pseudocapacitive material and it was discovered in 1971. In these devices charge storage involved storage of protons from electrolyte by faradaic reactions and electrodes exhibited a capacitor like behavior despite its faradaic nature. While the first experiments used single crystal RuO$_2$, bulk material only had up to 7% of Ru^{4+} atoms involved in redox reactions. Further experiments showed substantial increase in capacitance. Features that was engineered to increase capacity and enable fast redox reactions included [42];

i. Redox behavior of Ru^{4+} cations,
ii. Rapid electron transport provided by the metallic conductivity of RuO$_2$,
iii. Presence of structural water that allows proton transport within the inner surface,
iv. Decreased diffusion distances by obtaining larger outer surface area [42].

While these features were first studied for RuO$_2$, they are applicable to any other pseudocapacitive metal oxide, since similar properties define the capacitive behavior and energy storage mechanism of those materials.

Conducting polymers (CPs) can also store energy through redox reactions, making them suitable for supercapacitors as pseudocapacitive materials. CPs typically have low cost, high conductivity when doped, high voltage window, reversibility and are environmentally friendly [43]. Depending on the CP and its doped state, energy can be stored through ion pairing or delocalization of the charge; both requiring ion intercalation into the polymer chains [2]. Mechanism of doping of CPs can be seen below;

$$Cp \rightarrow Cp^{n+}(A^-)_n + ne^- \quad \text{(p-doping)}$$
$$Cp + ne^- \rightarrow Cp^{n-}(C^+)_n \quad \text{(n-doping)}$$
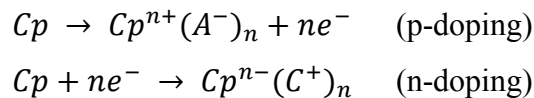
While CPs' potential window and capacitance is comparable to those of metal oxides, their swelling and shrinking during redox reactions, (namely intercalating and deintercalating processes) results in a much faster degradation compared to metal oxides [43]. Characteristic properties of some of the CPs when utilized as pseudocapacitor electrodes can be seen in Table 1.3.

Table 1.3 Characteristic properties of some CPs as electrode materials [41].

Conducting Polymer	Potential Range (V)	Conductivity $(S.cm^{-1})$	Theoretical Capacitance $(F.g^{-1})$
Polyaniline	0.7	0.1 – 5	750
Polypyrrole	0.8	10 – 50	620
Poly(3,4-ethylenedioxythiophene)	1.2	300 – 500	210
Polythiophene	0.8	300 - 400	485

In order to overcome the problem of morphological instability of CPs, they are generally utilized in nanocomposite form, which further increase their conductivity, capacitance or tune their morphologies to minimize shrinking and swelling during faradaic reactions. Thus, CPs are coupled with metal oxides, nitrides or ferrites [44–46], nanowires [47,48], graphene [49,50], carbon nanotubes [51], carbon fibers [52] or even with other CPs with different morphologies [53,54].

1.3   Electrode Materials

1.3.1   Carbon Materials

1.3.1.1 Activated Carbons

Carbon based materials have been used widely as supercapacitor electrodes because of their desirable physical and chemical properties on top of their low cost, processability and controllable porosity. Being the most abundant one, activated carbons (ACs) can be produced from carbon-rich natural or synthetic precursor materials through

carbonization in inert atmosphere. ACs are widely used because of its high surface area, moderate cost and easy fabrication and preparation [1]. Surface area of the ACs can be tailored up to 2500 m^2/g, yet some ACs with smaller surface area can provide better capacitive behavior up to 100 $F.g^{-1}$ [55,56].

1.3.1.2 Carbon Nanotubes

Carbon nanotubes (CNTs), are one of the carbon derivatives that have a novel structure with highly accessible surface area, very low resistivity and high electrochemical stability [57]. Both single walled carbon nanotubes (SWNTs) and multi walled carbon nanotubes (MWNTs) are studied extensively for supercapacitor devices [29,51,58,59]. SWNTs are wrapped up cylinders of one atom thick graphite (so called graphene) layers. Depending on the wrapping angle (Figure 1.7) they are classified as armchair, zigzag and chiral.
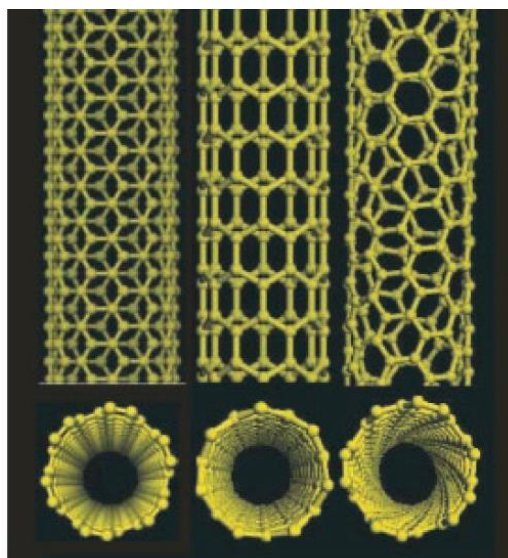
Figure 1.7 Different structures of SWNTs. From left to right, armchair, zigzag and chiral SWNTs [60].

12

Importance of CNTs for supercapacitor application arises from three characteristic properties,

    i.   Due to their tubular structures, CNTs have much better percolation than their other carbon-based counterparts,

    ii.   Ion diffusivity is much easier especially in composite form because of the entanglement, creating an open mesoporous network for active materials,

    iii.   High resilience of CNTs allow better cycling performance in the case of volumetric changes [57].

1.3.2   Metal Oxides

1.3.2.1 Ruthenium Oxide (RuO$_2$)

As mentioned in 1.1.2, RuO$_2$ was first discovered in 1971. RuO$_2$ stores energy with faradaic charge transfer reactions, yet showing capacitor like behavior in CV measurements. While theoretical specific capacitance of RuO$_2$ was found as 1450 Fg^{-1} from below reaction when $\delta=2$, subsequent studies obtained capacitance values around 700 Fg^{-1} using the structural water [61,62].

$$RuO_x(OH)_y + \delta H^+ + \delta e^- \leftrightarrow RuO_{x-\delta}(OH)_{y+\delta}$$
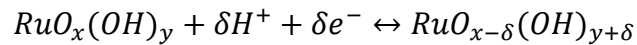
RuO$_2$ is one of the best canditate among other transition metal oxides due to its large potential window up to 1.2 V, which contains three highly reversible oxidation states, good thermal and chemical stability, good cycling performance and high proton conductivity. Charge transfer within RuO$_2$ is easy because of its quasi-metallic conductivity [43]. Moreover, hydrated RuO$_2$ reported to have better capacitance due to easier cation diffusion via hopping [63]. Yet, their high cost, possible toxicity to environment limited its use only to military appliances and prevented its widespread commercialization.

1.3.2.2 Manganese Oxide (MnO₂)

First research on pseudocapacitive behaviour of MnO_2 was conducted in 1999 on amorphous $MnO_2.nH_2O$ in aqueous KCl electrolyte, yielding a specific capacitance of approximately 200 Fg⁻¹ [64]. Other than RuO_2, only MnO_2 shows a capacitive behavior close to an ideal EDLC with a rectangular shape of CV among other transition oxides. Faradaic reactions of MnO_2 in aqueous electrolytes takes place through transition between its +4 and +3 oxidation states as shown below [42]:

$$MnO_2 + xA^+ + xe^- \leftrightarrow A_xMnO_2$$
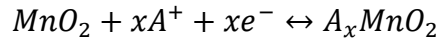
, where alkali metal cation is represented by A.

Theoretical specific capacitance of MnO_2 can reach up to 1300 Fg⁻¹ in addition to its abundancy, low cost and low toxicity all of which makes MnO_2 a good replacement for RuO_2. However, MnO_2 lacks the electronic conductivity of RuO_2 (electronic conductivity of RuO_2 is 10^4 S cm⁻¹ while that of MnO_2 is only 10^{-3} S cm⁻¹); while increased crystallinity makes up for the conductivity, it limits the proton exchange, hence lowering the capacitance [42,65]. Yet, studies on different MnO_2 structures reported gravimetric capacitances ranging from 200 to 850 Fg⁻¹ with aqueous electrolyte Na_2SO_4, proving that MnO_2 remains as a good replacement choice [66–68].

1.3.2.3 Nickel Oxide (NiO)

With high theoretical specific capacitance reaching up to 2600 Fg⁻¹, NiO received considerable attention as a supercapacitor electrode material [69]. It is considered to be an alternative electrode material in alkaline electrolytes for RuO_2 especially for its ease of synthesis and low cost. Energy is stored in NiO via faradaic reaction in a KOH electrolyte via the following reaction:

$$NiO + OH^- \leftrightarrow NiOOH^- + e^-$$

14
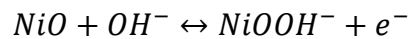
In spite of its high theoretical specific capacitance, problems such as poor cycle performance and high resistivity prevents supercapacitors based on NiO to obtain similar capacitance values [43]. To solve these problems, generally composites such as Co-Ni/Co-Ni oxides [70] or Co_3O_4-MnO_2-NiO ternary composite nanotubes [71] with highly porous mrphologies are formed.

1.3.2.4 Cobalt Oxide (Co_3O_4)

Oxides with spinel crystal structure offers three dimensional diffusion pathways. Being one of them, Co_3O_4 offers good supercapacitive behavior due to its intercalative pseudocapacitance provided by its unique structure on top of its large surface area, high conductivity, long term performance, environmentally friendliness, and good corrosion stability [43,72]. Co_3O_4 belongs to $Fd\overline{3}m$ space group, having cobalt ions with two different oxidation states, Co^{2+} and Co^{3+}, located at the interstitial tetrahedral and octahedral sites, respectively [73]. Representative structure of Co_3O_4 can be seen in Figure 1.8.
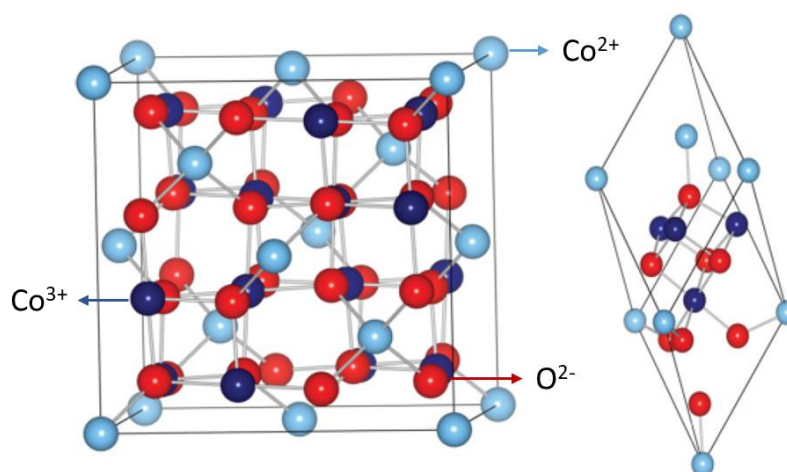
Figure 1.8 Cobalt oxide unit cell (left) and primitive cell (right), respectively [73].

Pseudocapacitance of Co_3O_4 in aqueous electrolyes originates from the faradaic reaction below [43],

$$Co_3O_4 + H_2O + OH^- \leftrightarrow 3CoOOH + e^-$$
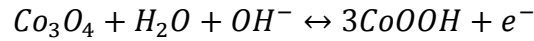
while its battery like properties due to Li^+ intercalation arises from below reaction [74],

$$Co_3O_4 + 8Li \leftrightarrow 4LiO_2 + 3Co$$
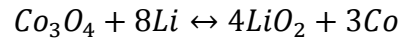
Even though Co_3O_4 shows a battery like behaviour, some studies have reported specific capacitances up to 700-800 Fg^{-1} [75,76], showing that Co_3O_4 is still a good candidate for EC electrodes.

1.4   Electrolytes

Capacitive behavior of the SCs are heavily depend on the electrolytes, depending on their ion size, ionic conductivity, voltage window and stability. Ion size of the electrolyte affects the performance directly depending of the ion accessibility through pores. Ionic conductivity is important for the overall internal resistance and charge transfer resistance of the supercapacitor devices. Moreover, energy and power densities of the SCs also depend on the voltage window of the electrolyte. While all of the aforementioned factors are very important for the commercialization of supercapacitors, their flammability, volatility and corrosion potential should also be low. Relationship between the electrolytes and their effect on the performance of supercapacitors can be seen in Figure 1.9.

Electrolytes can be grouped into five different categories, which are aqueous, organic, ionic liquid based, solid-state, and redox active electrolytes.
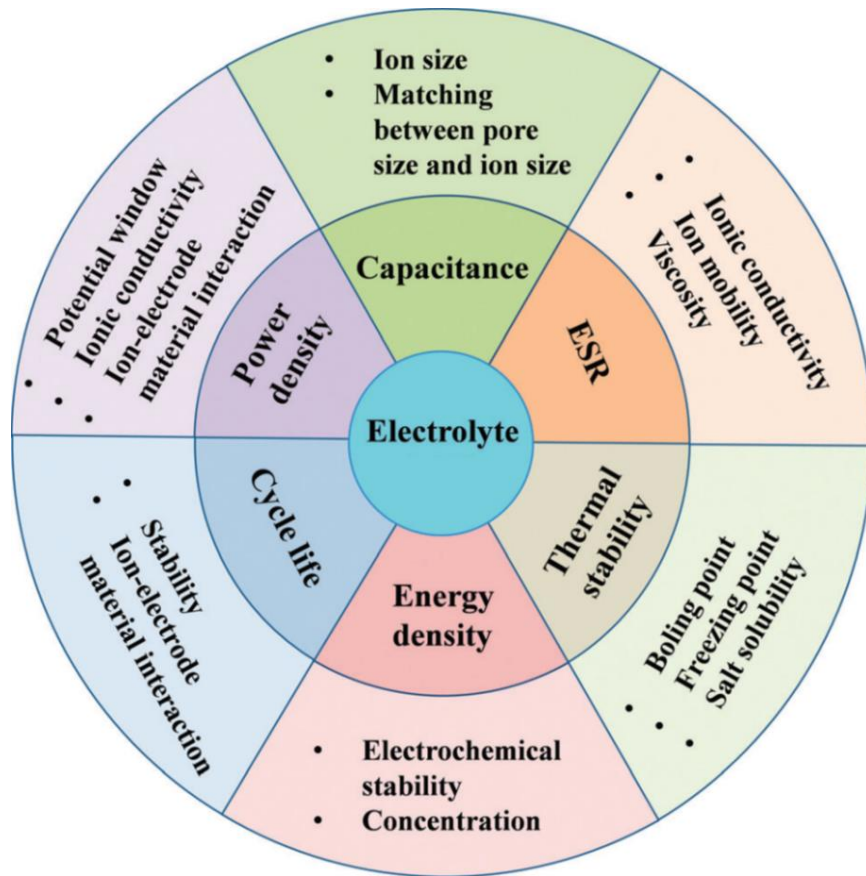
Figure 1.9 Sketch showing the relationship between electrolytes and their effect on electrochemical supercapacitors [77].

1.4.1 Aqueous Electrolytes

High ionic mobility and conductivity with low hazard levels are the main factors of preference for aqueous electrolytes especially in novel materials for supercapacitors. Yet, for commercial electrochemical supercapacitors, aqueous electrolytes are not preferred due to their low voltage window and leakage problem. Still, most of the research on supercapacitors are conducted using aqueous electrolytes, mainly due to their availability and low cost. Moreover, they do not need any special laboratory conditions such as moisture and oxygen level control; thus, can be used easily [77].

Acid, alkaline and neutral solutions are three subgroups that can be classified for aqueous electrolytes such as sulfuric acid (H_2SO_4), potassium hydroxide (KOH) and sodium sulfate (Na_2SO_4), respectively. With 0.8 $S.cm^{-2}$ ionic conductivity, H_2SO_4 exhibits much higher conductivity than organic or ionic liquid based electrolytes, resulting in a better equivalent series resistance (ESR) when utilized in SCs. However, possible hydrogen evolution at 0 V and oxygen evolution at 1.23 V (vs. standard hydrogen electrode (SHE)) restricts the use of aqueous electrolyte and shows possible threat to safety and performance decrease. For safety, potential window of aqueous electrolytes is limited to 1 V [77].

1.4.2   Organic Electrolytes

Organic electrolytes are generally preferred for commercial use because of their large potential window up to 2.8 V, which allows higher energy and power densities compared to aqueous electrolytes. Moreover, due to their low corrosivity, organic electrolytes allow cheaper materials to be used as substrates or current collectors in fabricated cells. Typical organic electrolytes include conducting salts such as tetraethylammonium tetrafluoroborate ($TEABF_4$), lithium perchlorate ($LiClO_4$) and lithium hexafluorophosphate ($LiPF_6$) dissolved in organic solvents such as acetonitrile or propylene carbonate (PC) [77].

While they are used widely within the products in the market, organic electrolytes have low ionic conductivity, high cost, possible flammability, volatility and toxicity. In addition, they require purification and controlled environment for the cell assembly. Furthermore, they result in lower specific capacitance.

1.4.3   Ionic Liquid Electrolytes

Composed of only ions of salts, ionic liquids (IL) are low temperature molten salts with melting points under 100 °C. ILs recently received extensive attention due to their high

18

ionic conductivity, high thermal, chemical and electrochemical stability and low volatility and flammability depending on the chosen cation and anion combination. Most important aspect of the ILs is that they can be engineered to meet conditions such as operating cell voltage, working temperature, ESR and electrochemical performance regarding to ion – electrode reactions by customizing the electrolyte composition. Typical cations for ILs are pyrrolidinium, ammonium and imidazolium while anions are tetrafluoroborate, hexafluorophosphate and dicyanamide [77].

ILs are reported to have a voltage window above 3 V, and even further up to 3.7 V if pyrrolidinium is used. Imidazolium based-ILs have low viscosity and high conductivity, thus in general imidazolium based ILs display higher power densities in SCs [78]. However, they are not sutable for room temperature use and are expensive. Thus the widespread use of Ils in SCs are limited.

1.4.4 Solid-State Electrolytes

Solid state electrolytes act as both ionic conductors and electrode seperators; realizing the growing demand for portable and flexible electronic devices. Solid-state electrolytes offer simple packaging and fabrication of supercapacitor devices as the fabricated device offers a liquid-leakage free design. Polymer-based solid electrolytes can be divided into two subgroups which are solid polymer electrolytes and gel polymer electrolytes (which is also called quasi-solid-state electrolyte due to presence of liquid phase). Solid-state electrolytes include polymer matrix such as poly(ethylene oxide) (PEO) and salt as lithium chlorde (LiCl), while gel polymer electrolytes include a polymer host such as polyvinylalcohol (PVA) and an aqueous electrolyte such as H_2SO_4. While gel polymer electrolytes have the advantage of having higher ionic conductivity than solid-states, they lack the mechanical strength and operating temperatures offered by solid-state electrolytes [77].

1.4.5 Redox-Active Electrolytes

Redox-active electrolytes induce pseudocapacitive behaviour to increase the capacitance of SCs through their own Faradaic reactions. These electrolytes generally consist of iodide species such as potassium iodide (KI). Although the use of redox-electrolytes is a simple and economic mean to obtain higher capacitance, there are still issues yet to be resolved. These include irreversibility of some redox species and migration of redox species between electrodes [79].

1.5 Electrochemical Measurements

1.5.1 Electrochemical Cell Desing

For electrochemical characterization of SCs, two electrochemical cell designs are present, namely three-electrode cell and two-electrode cell. Depending on the cell design, electrochemical measurements show different behaviour and accordingly the related calculations differ.

Three-electrode setup consist of a working electrode that is to be tested, a counter electrode, which is made from carbon such as a graphite rod or stable metals such as gold (Au) or platinum (Pt) and a reference electrode such as standard hydrogen electrode (SHE), saturated calomel electrode (SCE), and Ag/AgCl electrode in saturated potassium chloride (KCl). Purpose of three-electrode cell design is to obtain electrochemical information only on the working electrode. While the electrochemical measurement obtained from this setup does not represent the working electrode's condition in a full device, it gives insight on its performance and allows fast screening without the need for cell assembly [2].

Two-electrode setup, commonly referred as full device, consists of a positive and a negative electrode with active electrode surfaces. The use of same material in both electrodes result in a symmetric device, while different electrodes result in asymmetric

devices. A seperator wetted with electrolyte or solid electrolyte acting both as seperator and ionic conductor is used to seperate electrodes.

Gathering information on one electrode from a symmetric two-electrode setup is possible since the electrochemical behavior is expected to be same and total capacitance can be treated as sum of these two capacitances connected in series [2]. However, if an asymmetric cell is used, it is not possible to obtain data on an individual electrode. Moreover, if a symmetric pseudocapacitive SC cell is fabricated, redox activities are suppressed and are indistinguishable. Such an example can be seen in Figure 1.10, where a symmetric full device shows a rectangular cyclic voltammetry (CV) shape rather than showing any redox peaks.
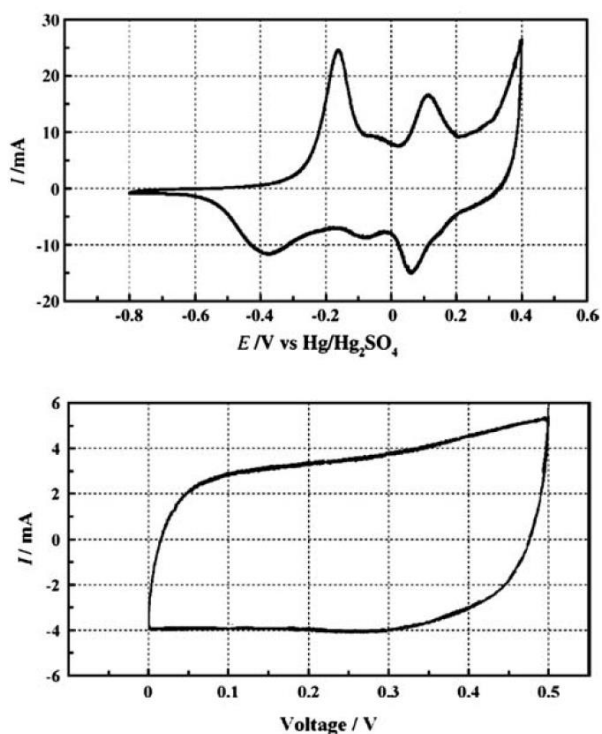
Figure 1.10 CV results of (top) three-electrode and (bottom) symmetric full device using polyaniline(PANI)/MWCNT electrodes [80].

1.5.2 Cyclic Voltammetry (CV)

CV is a potentiodynamic testing technique that provides kinetic analysis through scanning with a variable scan rate while providing qualitative and pseudo-quantitive analysis. It allows the determination of the potential or voltage window of the fabricated cell. Application of several scans also gives an insight on reversibility and reaction mechanisms on the surface of the electrode. Again, Figure 1.10 can be an example for the CV measurements for both three-electrode setup and full device cells having pseudocapacitive behaviour. Typical EDLC type CV curves can be seen in Figure 1.11.
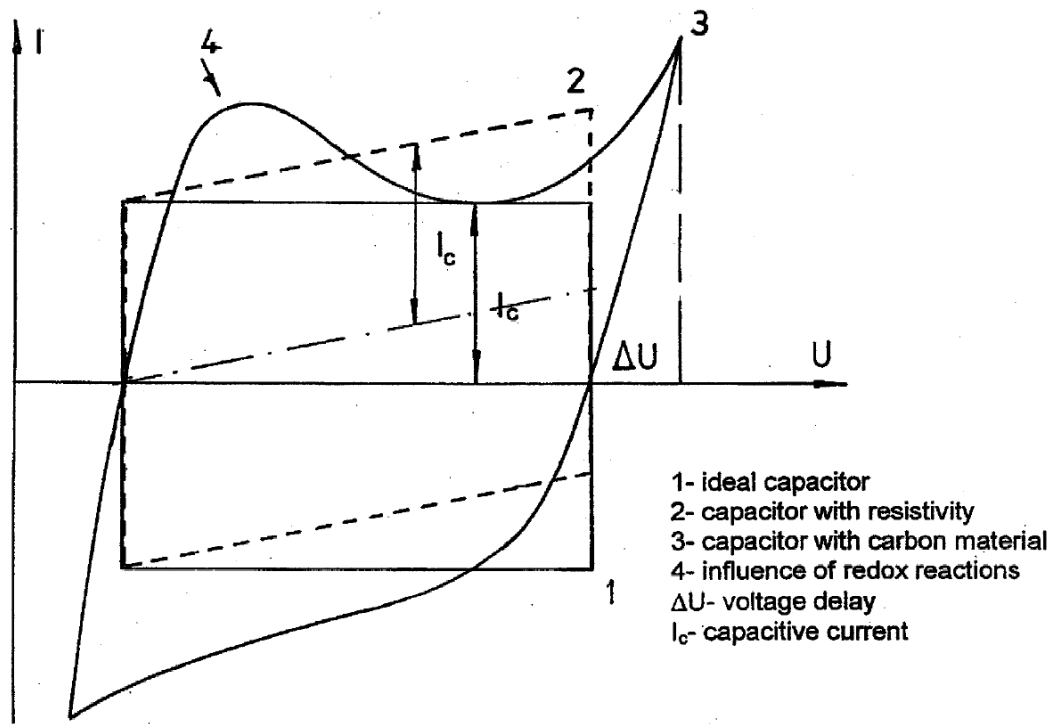
Figure 1.11 Typical CV curves for EDLC type electrochemical supercapacitors [55].

Electrode kinetics can be studied by applying different potential scan rates. If the scan rate is too fast, electrochemical reactions cannot follow electrode potential change. Dependence of the reaction kinetics on the scan rate can thus give qualitative and quantitative data [2].

22

One way to calculate specific capacitance from CV measurements is to use total charge transferred during scanning, Q, in the defined potential range E_1 to E_2 (V). If capacitance is expressed as C (F) then:

$$C = \frac{Q}{|E_2 - E_1|}$$

Charge obtained (Q) through CV scan can also be obtained by integration in which i (A) represents the measured current:

$$Q = \int_{t=0(E_1)}^{t(E_2)} i(E)dt$$

Thus, specific capacitance, C_{sp} $(F.g^{-1})$, can be obtained through the equation below:

$$C_{sp} = \frac{1}{m|E_2 - E_1|} \int_{t=0(E_1)}^{t(E_2)} i(E)dt$$

where m (g) is the mass of the active material of the working electrode. It is important to note that theoretically, the specific capacitance obtained from forward and backward scans in CV measurement must be same [2].

For a symmetric full device, capacitance obtained from CV measurement includes both electrodes. Total capacitance in this case becomes:

$$\frac{1}{C_T} = \frac{1}{C_p} + \frac{1}{C_n}$$

, where C_p and C_n represents capacitances of positive and negative electrodes, respectively. C_T represents the total capacitance of the full device that is calculated assuming these two capacitances are connected in series. In this case, C_p and C_n are equal to each other, resulting in a capacitance:

$$C = 2C_T$$

Thus, the C_{sp} equation becomes:

$$C_{sp} = \frac{1}{m|V_2 - V_1|} \int_{t=0(V_1)}^{t(V_2)} i(V)dt$$

, where V represents the cell voltage and V_1 to V_2 represents the voltage window of the cell. It should be noted that in this equation m represents the sum of the masses of two identical electrodes [2].

1.5.3 Galvanostatic Charge Discharge (GCD)

In galvanostatic charge discharge (GCD) measurements, a constant current is applied to the cell, while cell voltage is recorded with respect to the charging and discharging time. It is one of the most reliable electrochemical testing methods for the determination of capacitance, energy density, power density and cycle stability of the electrodes or full cell. While GCD can be applied both in three-electrode and two-electrode setups, making GCD measurements with two-electrode setup gives in more accurate results especially on the cycle life of the supercapacitor [1,2].

Voltage of the cell can be calculated according to the equation below (if the electrochemical leakage is negligible, where the resistance to leakage goes infinity) when charging:

24

$$V_{cell} = I_{cell}R_{esr} + I_{cell}\frac{t}{C_T}$$

, where V_{cell} is the cell voltage, I_{cell} is the applied constant current, and R_{esr} is the equivalent series resistance. Once the charging step is completed, discharging process starts immediately and voltage of the cell can be calculated as [1,2]:

$$V_{cell} = -I_{cell}R_{esr} + (V_{cell})_{max} - I_{cell}\frac{t}{C_T}$$

A typical GCD curve and related components from above equations is provided in Figure 1.12.
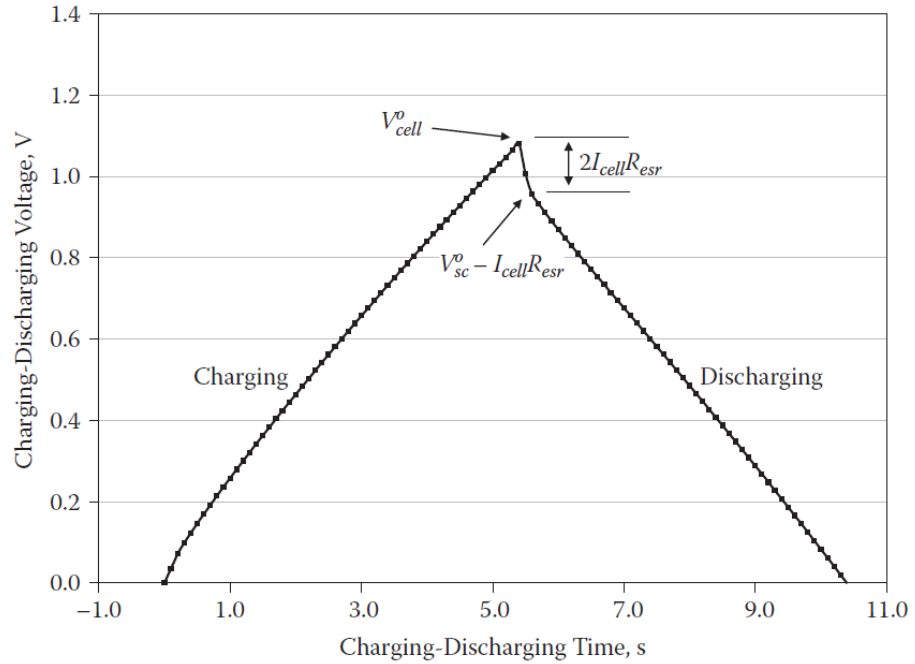
Figure 1.12 GCD curve of a symmetric supercapacitor cell with 3.8 mg.cm^{-2} carbon loading on 4 cm^2 stainless sheets with 0.0025 A.cm^{-2} current density using a 0.5 M Na$_2$SO$_4$ electrolyte [81].

Specific capacitance of the EDLC type of materials can be calculated from the discharge curve having a constant slope of the GCD curve:

$$C_{sp} = \frac{I}{m \frac{\Delta V}{\Delta t}}$$

, where I (A) is the current, ΔV (V) is the potential or voltage window, Δt (s) is the discharge time, and m (g) is the total mass of the active materials.

Discharge slope is not constant for pseudocapacitive materials because of their redox reactions. In such cases, capacitance of the cell can be calculated using the integral of the area under the curve to obtain discharge energy, E,

$$E = I \int_{t_i(V_{max})}^{t_f(V_{min})} V(t)dt$$

, where V (V) corresponds to the voltage window after IR_{drop}. From the discharge energy, capacitance of the cell can be calculated as:

$$C_T = \frac{2E}{V_{max}^2}$$

Here, C_{cell} correspods to a capacitance that includes mass of two serially connected identical electrodes. Thus, C_{sp} of an individual electrode can be calculated as [82,83]:

$$C_{sp} = 4C_T$$

Maximum power density P_{max} $(W.kg^{-1})$ and energy density E_{max} $(Wh.kg^{-1})$ of the fabricated cell can also be calculated using GCD curves using equations:

26

$$P_{max} = \frac{1}{4m} \frac{(V_{cell})^2_{max}}{R_{esr}}$$

$$E_{max} = \frac{1}{2} C_T (V_{cell})^2_{max}$$

GCD measurement is especially important for defining the cycle life of the supercapacitors. Degradation of cell can be monitored using GCD to charge and discharge the cell over many times to observe the loss of specific capacitance and increase in ESR. Theoretically, EDLC type SCs can have life cycles up to 100,000. However, degradation that occurs through charging and discharging cycles lowers both the energy and power density with time [2].

1.5.4 Electrochemical Impedance Spectroscopy (EIS)

Electrochemical impedance spectroscopy (EIS) or AC impedance spectroscopy has been developed for wet chemistry by Oliver Heaviside towards late 19th centuy. Nowadays, EIS is employed widely in the research especially on the characterization of batteries, fuel cells and supercapacitors for its ability to obtain information over an infinite frequency range by linear electrical perturbation and its experimental efficiency [84,85].

EIS gathers information through the analysis of electrical characteristics by employing a very small AC amplitude signals. For SCs, EIS can be applied within a large frequency range from 0.001 to 3,600,000 Hz, without effecting the characteristic properties of the electrode. Thus EIS is also defined as a non-destructive characterization technique.

Impedance is defined within linear systems theory and thus requires four important boundaries [85]:

i.   Linear equations must be used to describe response of the system,

ii.   System should relax to its initial state after AC perturbation is removed and hence the system must be stable,

iii.   System must not produce a response before perturbation is applied,

iv.   Impedance must be finite.

A linear relation between the current and the voltage exists when the applied AC perturbation is small enough, while the oscillating frequency is defined as:

$$\omega = 2\pi f$$
$$V = Z.I(V)$$

, where Z is the impedance, V is the voltage and I is the current. V and I can be expressed in detail as:

$$V(\omega) = \delta V exp(j\omega t)$$
$$I(\omega) = \delta I exp[j(\omega t + \phi)]$$

Hence, impedance can be expressed in ohms (Ω) as:

$$Z(\omega) = \frac{\delta V}{\delta I} exp(-j\phi)$$

, where $Z(\omega)$ is defined as complex impedance. This function with respect to oscillating frequency can also be defined as:

$$Z(\omega) = Z_{Re} + jZ_{Im}$$

, where Z_{Re} and Z_{Im} are the real and imaginary impedances, respectively. Phase angle in the function $Z(\omega)$ can be expressed using Z_{Re} and Z_{Im} as:

$$\phi = \arctan\left(\frac{Z_{Im}}{Z_{Re}}\right) \quad (°)$$

By these definitions, it is possible to linearize the complex electrochemical system and obtain an analogous electrical circuit that represents the electrochemical cell in hand. This *equivalent circuit* allows gathering information on the behaviour of the system and reaction kinetics [1]. One of the most basic circuit to represent basic electrochemical reactions, Randles equivalent circuit, and a model that includes both double layer and pseudocapacitance can be seen in Figure 1.13 (a) and (b), respectively. In the figures, R_s is equivalent series resistance, which corresponds to the resistance of the system containing electrolyte and electrode's resistance, R_{ct} is charge transfer resistance, W is Warburg diffusion component, or diffusion impedance which is due to ionic diffusion at the interface, C_{dl} is capacitance of the double layer, C_{ps} is capacitance of the pseudocapacitive material, and R_{leak} is resistance to possible leakage resistance. Warburg diffusion component in Figure 1.13 (a) is required in the case of fast adsorption kinetics [86].
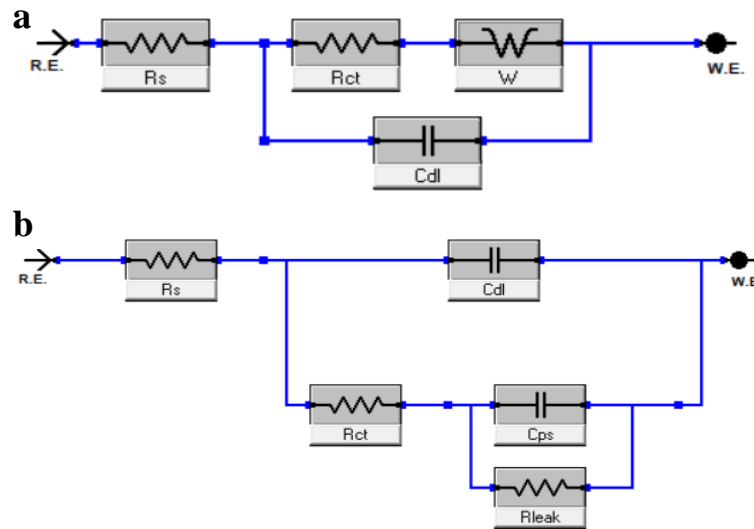
Figure 1.13 Equivalent circuit examples for EIS (a) Randles circuit and (b) circuit that contains pseudocapacitance in parallel with EDLC.

Nyquist plots, which are Z_{Im} vs Z_{Re}, are important to analyze supercapacitors' behavior. Typical Nyquist plots for EDLC and pseudocapacitive type of materials can be seen in Figure 1.14. At high frequencies, charge transfer resistance (R_{ct}) and double layer capacitance and at low frequencies, mass transport impedance is dominant.

Figure 1.14 (a) can be represented easily with R_s and C_{dl}, which are related with equivalent system resistance and charge accumulation at the electrode/electrolyte interface respectively. In ideal cases, capacitance should be constant over a range of frequencies; resulting in a vertical Nyquist plot [1].

Figure 1.14 (b), on the other hand, is typical behaviour of a pseudocapacitive material. Since the energy is stored through faradaic processes, kinetic rate constants which limit the mass transfer may exist. Of course, in a real case, electrode porosity and morphology could effect the impedance. Thus, resistances and capacitances are not constant with respect to frequency [1].
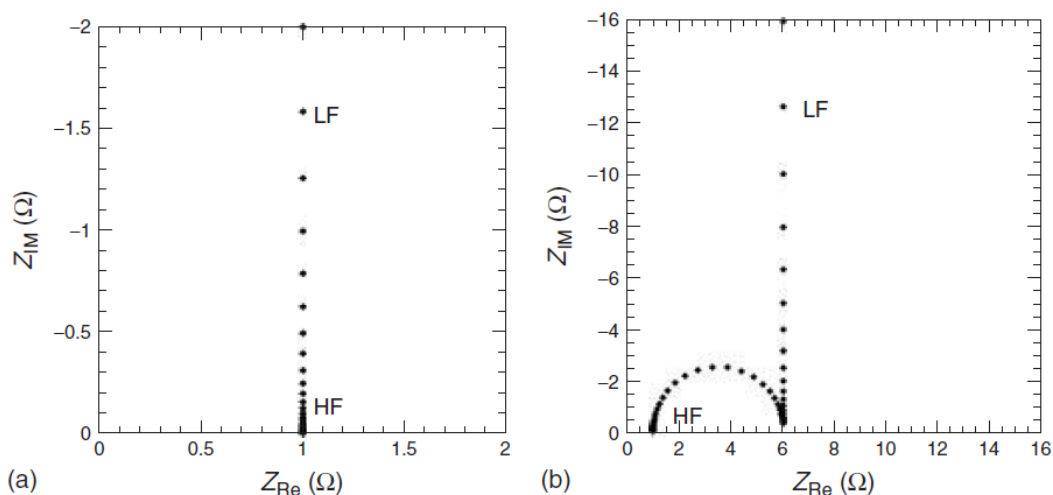
Figure 1.14 Nyquist plots of (a) ideal EDLC and (b) ideal pseudocapacitor [1]

1.6 Motivation of This Thesis

As discussed earlier, carbon materials are investigated extensively as SC materials especially due to their high conductivity and tunable specific surface area and pore structure. Being one of them, SWNTs offer excellent electrical conductivity and unique morphology.

Motivation of this thesis is to investigate the integration of physically and chemically modified SWNTs to the SCs as electrode materials. In Chapter 2, SWNT thin films are chemically modified through electrodeposition of Co_3O_4 to form nanocomposite thin film electrodes and influence of the SWNTs on the formation of the nanocomposite and the electrochemical performance of the fabricated nanocomposite thin film electrodes is investigated. In Chapter 3, binder-free SWNT buckypapers are physically modified by laser ablation to obtain micro-supercapacitor devices without any need for interdigitated contacts and their capacitive behavior is investigated.

CHAPTER 2

COBALT OXIDE NANOFLAKES ON SINGLE WALLED CARBON NANOTUBE THIN FILMS FOR SUPERCAPACITOR ELECTRODES

2.1 Introduction

ECs, which are also known as SCs, are highly appealing potential energy storage devices due to their high charge/discharge rates, long cycle life and high power density [5]. ECs have been known for almost 60 years with patents dating back to 1957 based on a capacitor utilizing the high surface area of carbon [3,4]. ECs attracted much more attention in recent years due to slow power delivery and uptake of Li-ion batteries [6]. The main concern in ECs is their low energy density, thus the recent research on supercapacitors is mainly focused on improving the energy density through the development of novel electrode active materials which also have high electrical conductivity, resistance to electrolyte corrosion and wide availability with low cost [87]. In fact, it is also possible to increase both energy and power density by increasing the charge accumulation and improving the charge transfer [88] through improving the electrode architecture using nanostructured materials such as nanowires [89], nanotubes [90] and nanorods [91]. This minimizes the diffusion length for ions and electrons [92].

There are two types of ECs based on their charge storage mechanism. First and the commercialized one is the EDLCs that are based on carbon as active materials and their charge storage mechanism arises from electrostatic attraction between ions and charged surfaces. Second is pseudocapacitors, in which charge storage is provided by electron-transfer mechanisms, namely faradaic reactions at the surface of the active materials such as transition metal oxides or conducting polymers [32]. RuO_2 based supercapacitors were extensively studied and reported to have specific capacitances above 700 F/g [93]; however, toxicity and high cost limited their widespread utilization. Instead, cheaper and environmentally friendly materials with similar

capacitive behavior were encouraged. Being one of them, Co_3O_4 was extensively investigated as an alternative material for supercapacitors due to its high pseudocapacitive properties. Co_3O_4 can be synthesized via various methods to be used in supercapacitors, such as electrodeposition [94–97], chemical growth [98–100], facile co-precipitation [101], rapid-microwave assisted synthesis [102], electrospinning [103], laser ablation in liquid [104] and hydrothermal synthesis [28, 29]. Moreover, fabricated Co_3O_4 were used in nanocomposite form, enhancing their capacitance and improving their structural integrity. Fabrication of Co_3O_4 nanocomposites with nickel foam [75,106,107], graphene [108], carbon nanotubes [109], copper foil [97], stainless steel foil [96] and ITO films [104] have been reported in this manner. Last but not least, several morphologies of Co_3O_4 was investigated with an intention to obtain better charge storage performance including core-shell structures [89,107,109], nanowires [75,89,106], nanoflakes [97], nanowalls [110] and nanoporous [111] structures. Among these morphologies of Co_3O_4, nanoflakes are the most promising one due to its large surface area and thin flake morphologies. Yet, research on the determination of the electrochemical potential of Co_3O_4 nanoflakes on SWNT thin films in organic electrolytes remained elusive.

In this study, we present a novel and an easy route for the fabrication of Co_3O_4/SWNT nanocomposite thin film electrodes on glass substrates. SWNT thin films are used as the current collectors for EC electrodes instead of conventional metal foils and the use of organic electrolytes provided a wider potential range in anodic region compared to the extensively reported window with potassium hydroxide. Structural and electrochemical characterizations of the nanocomposite thin films are followed by detailed morphological analysis conducted through transmission electron microscopy (TEM) in conjunction with galvanostatic charge/discharge cycles.

2.2 Experimental Section

2.2.1 Materials

SWNTs used in this study was purchased from Carbon Solutions (P3-SWNT) with a diameter and length of 1.55 nm and 500 nm, respectively. Sodium dodecylbenzenesulfonate (SDBS) and cobalt (II) nitrate hexahydrate ($Co(NO_3)_2.6H_2O$, ACS reagent $\geq$ 98 %) are obtained from Sigma-Aldrich. Nitrocellulose filter membranes (GSWP, 0.22 µm pore size) are purchased from Merck Millipore. All materials are used without further purification.

2.2.2 Preparation of SWNT Thin Films

SWNT thin films are prepared using vacuum filtration and consecutive stamping method [37, 38]. They are utilized as both current collectors and EDLC on the glass substrates. For the preparation of thin films 1wt % of SDBS (as dispersant) is dissolved in 250 mL of DI water (18.3 MΩ-cm) using tip sonication for 10 minutes. Afterwards, 1.5 mg of SWNTs are added to the solution and tip sonication is conducted for additional 10 minutes. 20 mL of the as prepared solution is vacuum filtrated with a rate of 18 mL/min.cm² onto filter membranes, which corresponds to a SWNT weight of 0.06 mg.cm^{-2}. Deposited SWNT films on filter membranes are rinsed with deionized water to remove excess SDBS. Glass substrates were cleaned via sonication in acetone, isopropanol and deionized water for 15 minutes each followed by an oxygen plasma treatment for 5 minutes (Femto Science CUTE). SWNT filtrated membranes are placed onto cleaned glass substrates, compressively loaded (5 N.cm^{-2}) and dried for 2 hours at 80 °C. After drying, filter membranes are dissolved and washed with acetone to dissolve the membrane, leaving SWNT thin films over an area of 2 cm^2 on glass substrates. SWNT thin films are further cleaned with acetone and isopropanol to remove remnants of the membrane and SDBS. Additional cleaning is conducted by soaking SWNT thin films into 50%

nitric acid (HNO$_3$, 65%) solution, which also improved the conductivity of SWNT thin films [114]. Films are rinsed with water and dried following the acid treatment. External contacts are painted using a conductive carbon paint.

2.2.3 Fabrication of Nanocomposite Thin Film Electrodes

A 0.05 M solution of Co(NO$_3$)$_2$.6H$_2$O is freshly prepared for electrodeposition using platinum foil as the counter electrode and Ag/AgCl in saturated KCl solution as the reference electrode. Gamry Reference 3000 is used as potentiostat/galvanostat system for the electrodeposition process. Co(OH)$_2$ is electrodeposited onto SWNT thin films using CV between a potential range of 0 to -1.2 V for 30 cycles at a scan rate of 20 mV/s. Electrodeposition is conducted at room temperature and the glass substrates are rinsed with DI water at the end of the electrodeposition. Fabricated Co(OH)$_2$/SWNT samples are annealed in air at 190 °C to form Co$_3$O$_4$/SWNT nanocomposite electrodes and used in electrochemical analysis without any further process.

2.2.4 Characterization of the Fabricated Thin Film Electrodes

X-ray photoelectron spectroscopy analysis (XPS) and Raman spectra of bare SWNT thin films and Co$_3$O$_4$/SWNT nanocomposite electrodes are collected via PHI 5000 VersaProbe spectrometer and HORIBA Jovin Yvon iHR550 (laser wavelength of 532 nm), respectively. Charge corrections and binding energies of corresponding bonds are referenced to the C (1s) at 284.5 eV. Morphology and the structure of the thin film electrodes are characterized by scanning electron microscopy (SEM) using a FEI Nova Nano SEM 430 microscope (operated at 10 kV). SEM samples are prepared through gold sputtering prior to the analysis to prevent charging caused by the glass substrate. Further structural analysis is performed by TEM using a JEOL TEM 2100F microscope (operated at 200 kV). For the preparation of TEM samples, nanocomposites are scraped off the substrate, sonicated in ethanol and drop casted onto TEM grids.

Electrochemical characterization of the electrodes was performed using a Gamry Reference 3000 potentiostat/galvanostat system in three-electrode configuration under ambient conditions. Ag/AgCl in saturated KCl and platinum foil are used as the reference and counter electrodes, respectively. All potentials are relative to the Ag/AgCl reference electrode. 1 M lithium perchlorate (LiClO$_4$) in propylene carbonate (PC) is used as the electrolyte solution for electrochemical measurements. CV, galvanostatic charge-discharge curves (GCD), and potentiostatic electrochemical impedance spectroscopy (PEIS) methods are used for the analysis of electrochemical behavior of the fabricated thin films. A Sartorius Research R200D microbalance is used to measure the mass of the deposited cobalt oxide as the active material, which was approximately 0.12 mg.cm^{-2} per electrode.

2.3   Results and Discussion

2.3.1   Formation of Nanocomposite Thin Films

Fabrication of Co$_3$O$_4$/SWNT thin film electrodes are simply achieved by electrodeposition of Co(OH)$_2$ onto vacuum filtrated SWNT thin films via CV within a potential window of 0 to -1.2 V at a scan rate of 20 mV/s. This is followed by calcination to obtain Co$_3$O$_4$. CV curves obtained during the deposition of Co(OH)$_2$ on SWNT thin films for 30 cycles are shown in Figure 2.1 (a). Voltammogram gets narrower as the deposition proceeds, indicating that the amount of Co(OH)$_2$ deposited decreases on each cycle since the surface area of SWNT decreases gradually with continuous nucleation and growth of Co(OH)$_2$, decreasing the number of available nucleation sites.
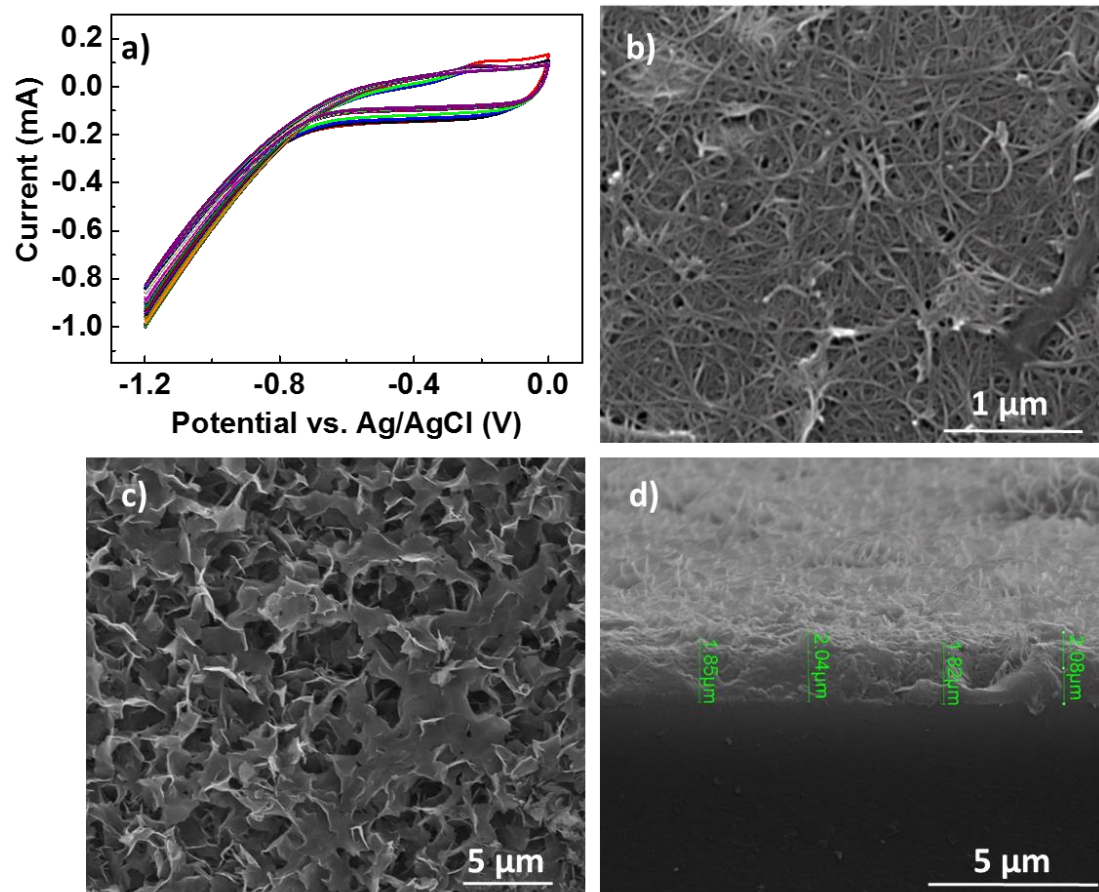
Figure 2.1 (a) CV curves obtained during the deposition of Co(OH)$_2$ on SWNT thin films. Top view SEM images of (b) bare SWNT thin film, (c) Co$_3$O$_4$/SWNT thin film and (d) cross-sectional SEM image of Co$_3$O$_4$/SWNT thin film [115].

Reactions governing the formation of Co(OH)$_2$ layer is given as [95],

$$2H_2O + 2e^- \rightarrow H_2(g) + 2OH^- \qquad (1)$$

$$Co^{2+} + 2OH^- \rightarrow Co(OH)_2 \qquad (2)$$
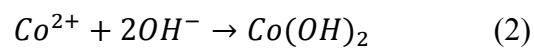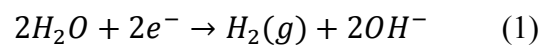
First reaction is associated with the evolution of hydrogen while the latter shows the formation of $Co(OH)_2$ with the reaction of Co^{2+} ions and hydroxyl groups formed during the first step. At the end of 30 cycles, $Co(OH)_2$/SWNT thin films are washed with DI water and dried at 50 °C under ambient conditions for 1 hour. Dried $Co(OH)_2$/SWNT thin films are then calcined in air at 190 °C to obtain Co_3O_4/SWNT nanocomposite thin films. Calcination reaction can be given by [116]:

$$3Co(OH)_2 + \frac{1}{2}O_2 \rightarrow Co_3O_4 + 3H_2O \qquad (3)$$
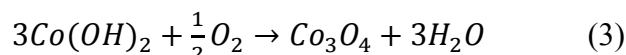
2.3.2   Characterization of Nanocomposite Thin Films

Morphology of the fabricated Co_3O_4/SWNT nanocomposite thin films on glass substrates are investigated through top view and cross-sectional SEM images, which are provided in Figure 2.1 (b)-(d). SEM images reveal the porous nanoflake structure, which would facilitate ionic transport [19,117]. Cross-sectional SEM image provided in Figure 2.1 (d) show a uniform thickness of about 1.95 μm for the nanocomposites, demonstrating a uniform growth of Co_3O_4 on SWNTs via electrodeposition. TEM analysis is conducted both for the as prepared and electrochemically cycled (1500 and 3000) thin films in order to monitor the morphological and structural stability of the Co_3O_4 nanoflakes during cycling. d-spacing values (Table 2.1) are calculated from the selected area electron diffraction (SAED) patterns in TEM images (Figure 2.2 (c), (f) and (i)) using Gatan Digital Micrograph 3 software. These experimentally obtained d-spacing values clearly indicate that the obtained oxide is Co_3O_4 (JCPDS card no 42-1467). It is evident from the TEM images that the electrochemically deposited $Co(OH)_2$ and progressively obtained Co_3O_4 is textured. SWNTs might be the reason for this texturing, since the number and the orientation of available nucleation sites for Co_3O_4 nanoflakes strongly depend on the walls of SWNTs.

Table 2.1 Experimentally determined d-spacing values obtained from TEM diffraction using Gatan Microscopy [115].

No	Plane group	Asprepared Co_3O_4/SWNT thin film d-spacing (Å)	After 1500 cycles d-spacing (Å)	After 3000 cycles d-spacing (Å)
1	{111}	4.76	4.77	4.74
2	{202}	2.92	2.92	2.86
3	{113}	2.47	2.46	2.43
4	{222}	2.38	Not observed	Not observed
5	{004}	2.06	2.07	2.02
6	{224}	1.68	1.69	Not observed
7	{333}	1.58	1.57	1.55
8	{044}	1.45	1.45	1.43
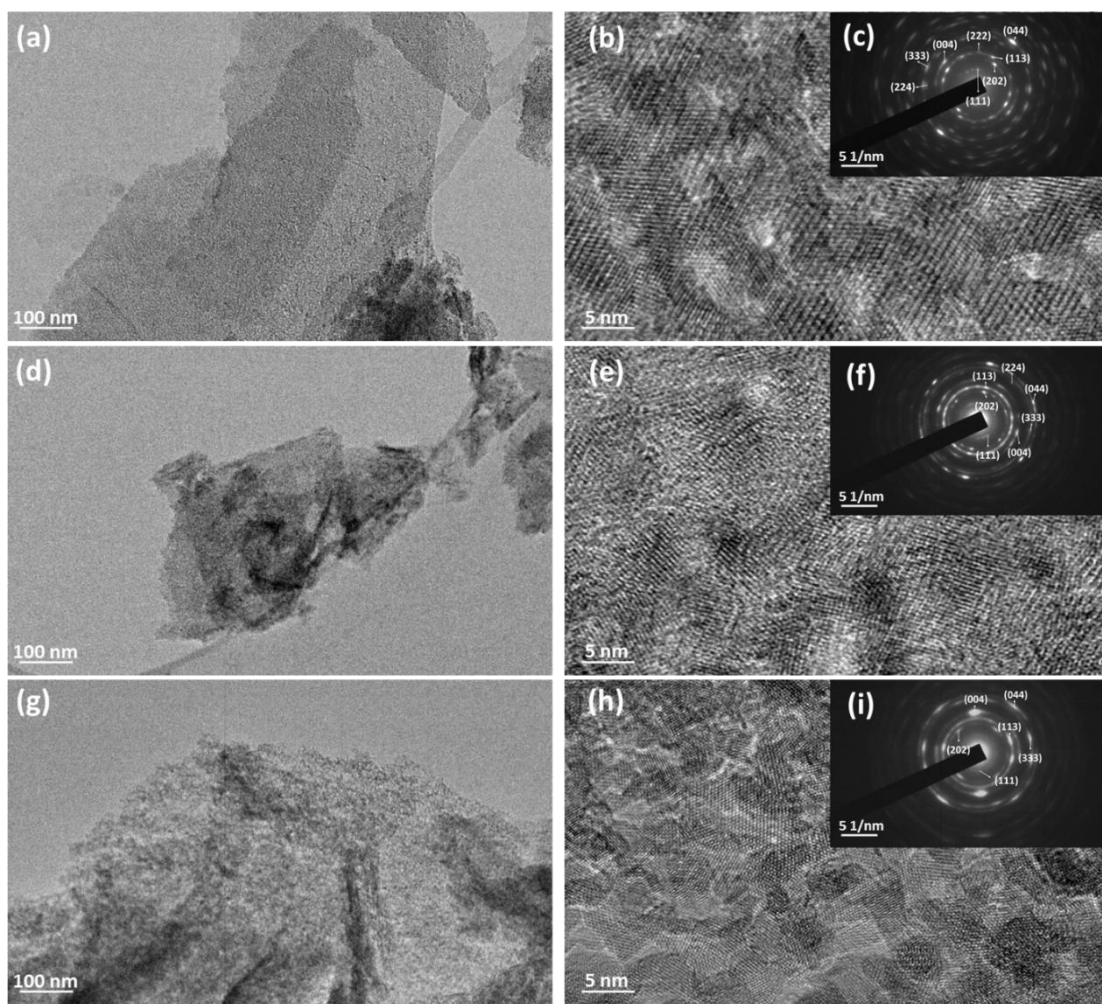
Figure 2.2 TEM images of prepared, galvanostatically 1500 times and 3000 times charged and discharged Co_3O_4/SWNT nanocomposite thin film electrodes at (a), (d), (g) low magnification, (b), (e), (h) high magnification and (c), (f), (i) corresponding SAED pattern with identified planes, respectively [115].

For detailed chemical analysis of the fabricated electrodes, XPS analysis was conducted and results of which are provided in Figure 2.3 (a)-(c). Figure 2.3 (a) shows the XPS survey of Co_3O_4/SWNT nanocomposite thin film and bare SWNT thin films in which position correction was done with respect to C 1s peak. According to Figure 2.3 (a), Co_3O_4/SWNT nanocomposite have signals at 779.6 – 794.5, 529.6 and 284.5 eV, which were attributed to the Co 2p, O 1s, and C 1s signals. As shown in the Figure 2.3 (b), spin orbit peaks in the high resolution XPS spectrum for Co $2p_{3/2}$ and Co $2p_{1/2}$ are observed at 779.6 and 794.5 eV, respectively, which are found to be in good agreement with the previous studies [118]. Absence of the satellite peaks caused by the mixed state of oxides confirmed the total transformation to Co_3O_4 upon annealing [119]. Figure 2.3 (c) shows the high resolution XPS spectrum of O 1s, which corresponds to O^{2-} ions in the crystal structure of Co_3O_4 [118]. Moreover, atomic percentages of C, Co and O were obtained from XPS survey as 15.5, 37.0 and 47.6%, respectively. Atomic percentages of Co and O also matches with the atomic structure of Co_3O_4, further confirming that the obtained structure is Co_3O_4 [115].

To further investigate the chemical nature of the Co_3O_4/SWNT nanocomposite films, Raman spectroscopy was conducted. Figure 2.3 (d) shows the Raman spectrum of both bare SWNT thin film and Co_3O_4/SWNT nanocomposite film within the spectral range of 300 – 1700 cm^{-1}. Absence of the D-band and high intensity of the G-band suggests the high crystallinity of SWNTs as well as showing that there are no defective SWNTs present within thin films. As expected, porous nature of supposedly absorbing Co_3O_4 nanoflakes allowed the observation of G-band of SWNTs even though, as evidenced by SEM, Co_3O_4 nanoflakes totally cover SWNT films. Peaks at 482, 523, 620 and 689 cm^{-1} are attributed to crystalline Co_3O_4, namely to E_g, F^1_{2g}, F^2_{2g} and A_{1g} modes, respectively [120].
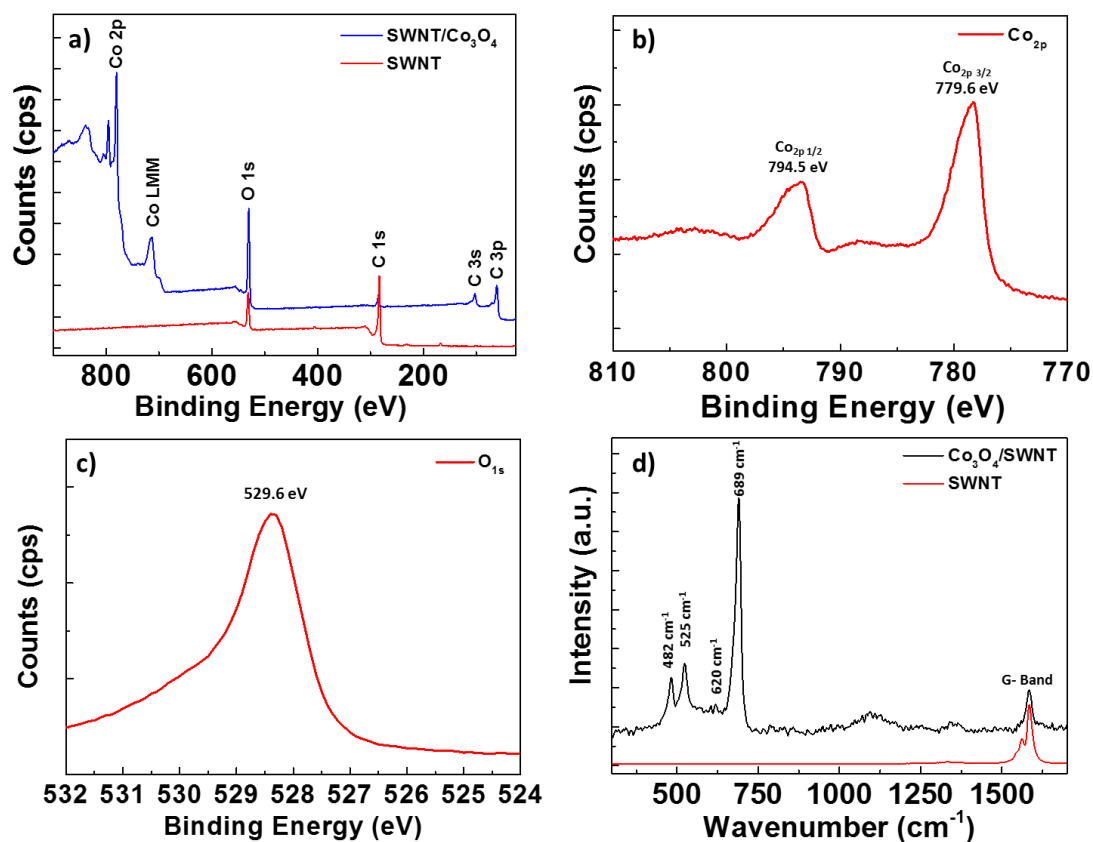
Figure 2.3 (a) XPS survey spectrum of bare SWNT thin film and Co_3O_4/SWNT nanocomposite thin film. High resolution XPS spectrum of Co_3O_4/SWNT thin film showing (b) Co 2p and (c) O 1s spin orbits. (d) Raman spectra of bare SWNT thin film and Co_3O_4/SWNT nanocomposite film [115].

2.3.3   Electrochemical Characterization

CV is used to evaluate the electrochemical performance of the fabricated supercapacitor electrodes. CV characteristics of bare SWNT and Co_3O_4/SWNT nanocomposites within a potential window of $0 – 1.2$ V are provided in Figure 2.4 (a). SWNT has dual character and it is utilized as both current collector and an electric double layer capacitor. Figure 2.4 (a) shows evident improvement in the charge storage performance by the presence of Co_3O_4 on SWNT thin films. This also shows that the SWNT has a limited contribution to charge storage and Co_3O_4 nanoflakes mainly supply charge storage. The potential window is particularly chosen and beyond 1.2 V, a non-reversible reaction occurs, preventing wider potentials in anodic region. We have also investigated negative potentials; however, since the Co_3O_4 is an anodic electroactive material, results obtained only in a potential window of 0 to 1.2V is reported here. Furthermore, different number of deposition cycles (10, 20, 30 and 40 cycles) of Co_3O_4 was also applied to obtain samples with different thicknesses. Comparison of the CV results and charge-discharge curves can be seen in Figure 2.5 (a) and (b), respectively. While there is evident improvement in the charge storage capacity up to 30 cycle of deposition, performance stays constant in the nanocomposite with the next 10 cycles of deposition (40 cycles in total). This is probably because of the deceleration of $Co(OH)_2$ electrodeposition during the last 10 cycles and it did not change the amount of deposited active material seriously. Moreover, large number of deposition cycle may result in the blockade of pores and it may limit the diffusion of electrolyte ions to inner sides of the nanocomposite electrodes. Herein only the Co_3O_4/SWNT nanocomposite electrodes with best performance is elaborated, which corresponds to 30 deposition cycles. Electrochemical performance of the nanocomposite electrodes prior to annealing is provided both in terms of CV and GCD in Figure 2.6 (a) and (b), respectively. Although electrodeposited $Co(OH)_2$ shows enhanced capacitive performance compared to bare SWNTs, annealing and conversion to Co_3O_4 improved the performance approximately by 10 times [115].
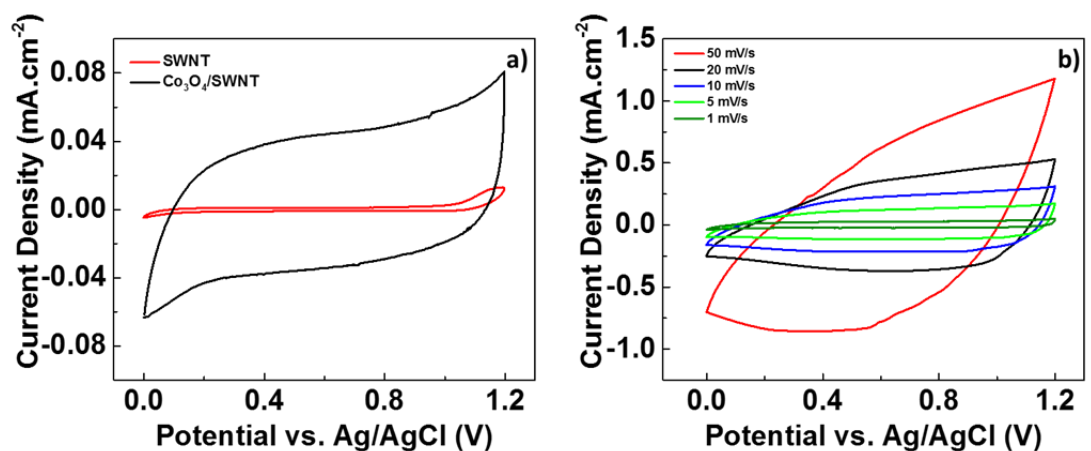
Figure 2.4 (a) CV results of bare SWNT thin film and Co₃O₄/SWNT nanocomposite at a scan rate of 1 mV/s in 1M LiClO₄ in PC electrolyte solution and (b) CV curves of Co₃O₄/SWNT nanocomposite electrode at different scan rates [115].
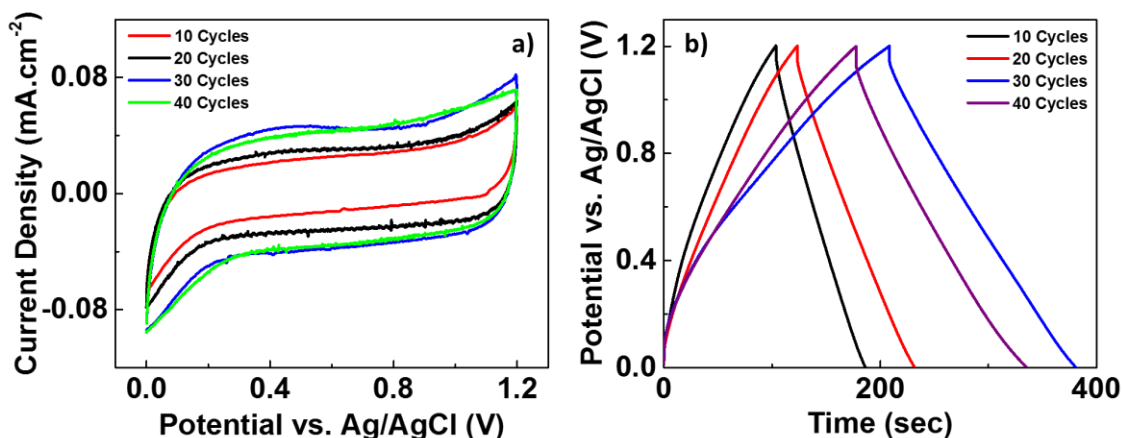
Figure 2.5 Electrochemical comparison of Co₃O₄/SWNT nanocomposite electrodes with different amount of deposited cobalt oxide by applying varying number of cycles during electrodeposition. (a) CV curves at a scan rate of 1 mV/s and (b) GCD results at a current density of 125 µA.cm⁻² [115].
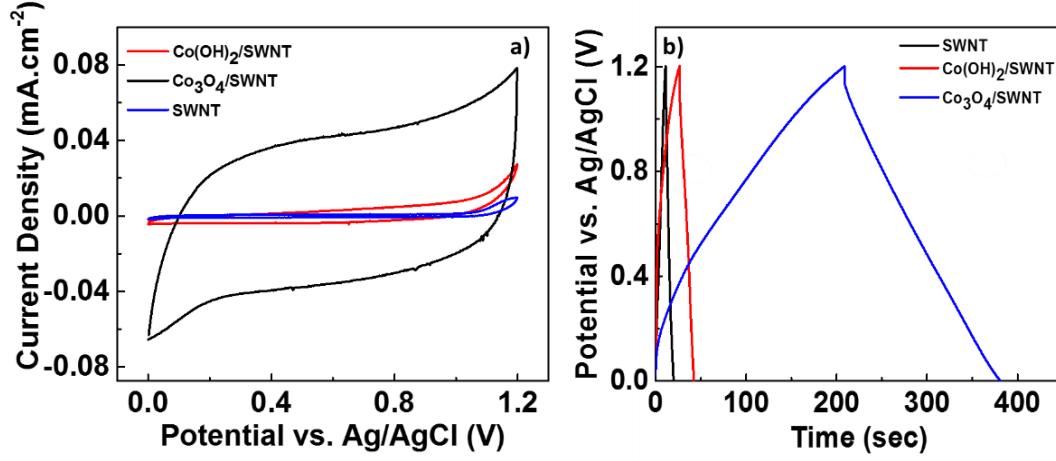
Figure 2.6 (a) CV curves of bare SWNT, Co(OH)$_2$/SWNT and Co$_3$O$_4$/SWNT electrodes at 1 mV/s scan rate and (b) GCD curves of SWNT, Co(OH)$_2$/SWNT and Co$_3$O$_4$/SWNT electrodes at a current density of 125 μA.cm^{-2} [115].

CV measurements of the fabricated Co$_3$O$_4$/SWNT nanocomposite electrodes were also conducted with different scan rates. Figure 2.4 (b) shows CV curves of Co$_3$O$_4$/SWNT nanocomposites with scan rates ranging from 1 to 50 mV/s. It is seen in the figure that the nanocomposite electrodes preserved their curve shapes at higher scan rates. This showed that the fabricated electrodes have good rate capability.

Specific capacitance values of the prepared nanocomposite electrodes are calculated using the CV curves in the Figure 2.4 (b) according to the following formula:

$$C_{sp} = \int \left(i(E)dE \middle/ 2V(E_2 - E_1)m \right) \quad (5)$$

,where C_{sp} is the gravimetric capacitance (F.g^{-1}), $i(E)$ is the instantaneous current (A), $\int i(E)dE$ is the total charge obtained from the integral of voltammogram, $(E_2\text{-}E_1)$ is the potential window width (V) and m is the mass of the active material (g). Calculated

46

specific capacitances for, the Co_3O_4/SWNT nanocomposite electrodes are 313.9, 181.7, 160.4, 124.2 and 89.1 $F.g^{-1}$ for the scan rates of 1, 5, 10, 20 and 50 mV/s, respectively [115]. Ionic migration in the electrolyte is diffusion limited, resulting in a decrease in the specific capacitance at higher scan rates [104]. Areal capacitance values of the electrodes are also calculated using the following formula:

$$C_{sp} = \int \left(i(E)dE \Big/ 2V(E_2 - E_1)A \right) \quad (6)$$

, where A is the area of the fabricated thin film electrodes on the glass substrate (in cm^2). Prepared circular thin films had an area of 2 cm^2. The areal capacitances of the electrodes were 70.5, 40.8, 36.0, 27.9 and 20.0 $mF.cm^{-2}$ for scan rates of 1, 5, 10, 20 and 50 mV/s, respectively [115]. Absence of the distinct redox peaks in CV curves indicates that the obtained porous nanoflake structure allow Li^+ storage only on the surface of the nanocomposite, resulting in a ideal capacitor like behaviour [12].

Specific capacitance changes with respect to scan rates are provided in Figure 2.7 both for gravimetric and areal capacitances. Specific capacitance values decreased with increasing scan rates due to the diffusion limited charge storage mechanism, which is even more drastic in organic electrolytes since their ionic conductivities are much lower than the aqueous counterparts [77].
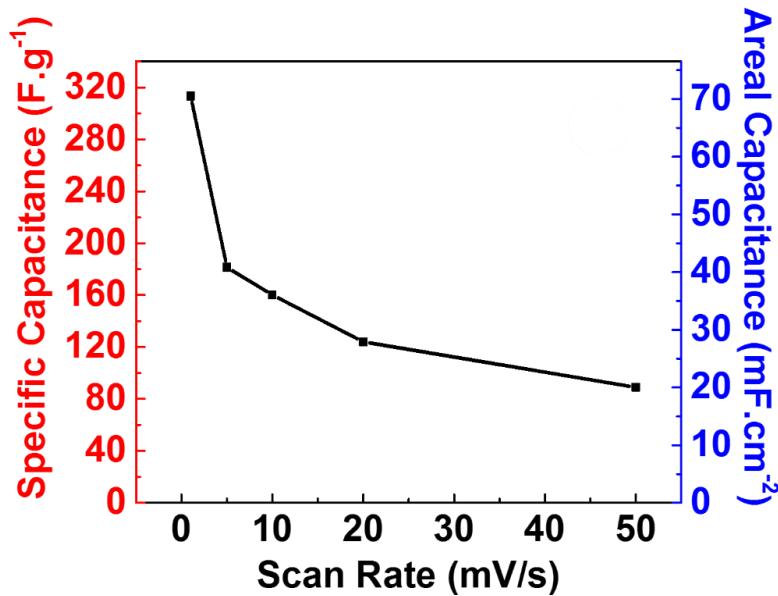
Figure 2.7 Specific capacitances of Co_3O_4/SWNT nanocomposite electrodes with respect to scan rates. Lines are included for visual aid [115].

Figure 2.8 (a) shows the GCD of bare SWNT thin films and Co_3O_4/SWNT nanocomposite electrodes measured at a current density of 50 $\mu A.cm^{-2}$. It is clearly seen in the figure that the Co_3O_4/SWNT nanocomposite electrodes have longer charge-discharge times than the bare SWNT electrodes with an improved charge storage property. Similar to CV measurements, deposition of Co_3O_4 nanoflakes extensively improved GCD curves with their pseudocapacitive properties. This indicates that the Co_3O_4 have a superior pseudocapacitive property. GCD measurements for Co_3O_4/SWNT nanocomposite electrodes were also conducted with different current densities ranging from 50 $\mu A.cm^{-2}$ to 500 $\mu A.cm^{-2}$ and it is provided in the Figure 2.8 (b). Fabricated nanocomposite electrodes have a very limited initial internal resistance drop and it might be due to the high conductivity of the SWNT films and the improved charge transfer between the Co_3O_4 nanoflakes and the SWNT thin films. It is also observed that the discharge profiles are affected with the applied current density. As such, decreasing the applied current density greatly enhanced the coulombic efficiencies. For current densities of 500, 250, 100, and 50 $\mu A.cm^{-2}$, coulombic efficiencies are calculated as 73, 78, 80 and 89%, respectively [115]. This shows that

Co₃O₄/SWNT nanocomposite electrodes have excellent charge/discharge performances at low current densities.
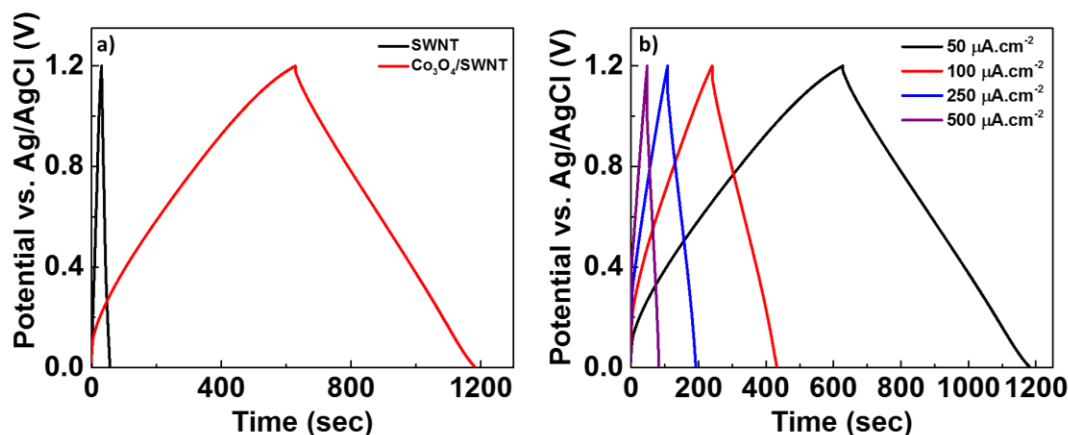
Figure 2.8 (a) Comparison of GCD performances of bare SWNT films and Co₃O₄/SWNT nanocomposite electrodes at a current density of 50 µA/cm^{-2} and (b) Co₃O₄/SWNT nanocomposite electrodes at different current densities [115].

Electrochemical behavior of the Co₃O₄/SWNT nanocomposite electrodes are further evaluated by EIS within a frequency range of 100 kHz to 0.01 Hz. For the EIS measurements, an AC perturbation of 5 mV is used under different DC potentials. Co₃O₄/SWNT nanocomposite electrodes are compared under different DC potentials of 0 V (open circuit), 400 and 800 mV and the corresponding EIS plot is provided in Figure 2.9 (a). Since Co₃O₄ is an anodically electroactive material, with an increase in the applied positive bias, equivalent resistance of the system is decreased due to a decrease in the charge transfer resistance. This can be clearly seen in the provided Nyquist plot. While the open circuit model is highly diffusion limited in the low frequency region, applied bias increases the diffusion rate, which increase the slope of the straight line, showing an ideal supercapacitive behavior. Figure 2.9 (b) shows the Nyquist plot of the prepared Co₃O₄/SWNT nanocomposite electrode with the respective equivalent circuit. Fabricated nanocomposite electrodes have a porous

structure and it needs a complex circuit model to fit the obtained data. EIS model is used to determine different electrode parameters (Figure 2.9 (b)), such as equivalent series resistance (R_{eq}), charge transfer resistance (R_{ct}), mass capacitance (C_{mass}), Warburg element (W_d), resistance to leak (R_{leak}) and capacitance of the electrode (C_{cap}) at an applied bias of 800 mV. R_{eq} of the system is determined as 54 Ω, while R_{ct} is 26 Ω [115]. Both resistances are mainly due to use of an organic electrolyte. The distorted semicircle within the high frequency region is a result of these relatively high R_{eq} and R_{ct}.
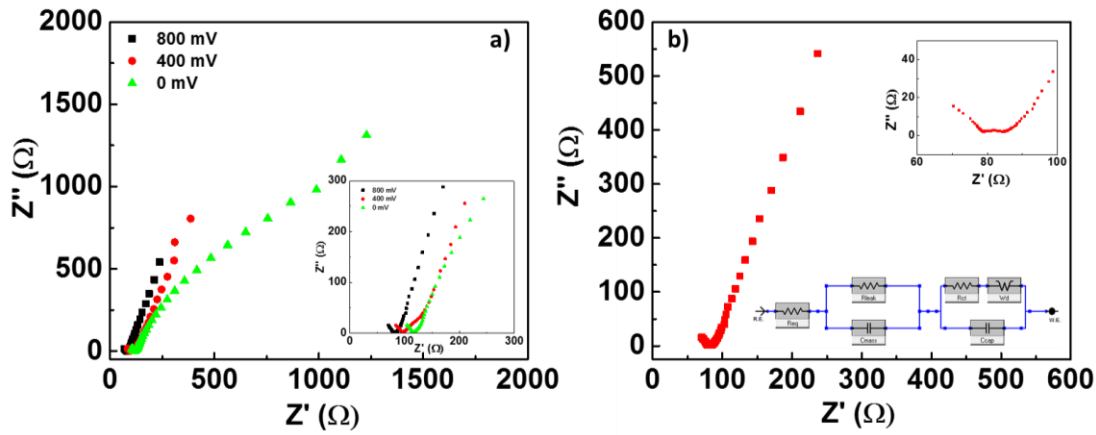
Figure 2.9 (a) EIS spectra of Co_3O_4/SWNT thin films at different applied DC potentials and (b) EIS spectrum of Co_3O_4/SWNT thin films and its related circuit model (R_{eq}: equivalent resistance of the system, R_{ct}: charge transfer resistance, R_{leak}: leakage resistance, W_d: Warburg element, C_{mass}: capacitance related with mass, and C_{cap}: capacitance of the thin film) [115].

As another important electrochemical performance parameter, capacity retention of the Co_3O_4/SWNT nanocomposites is also determined with constant charge-discharge cycles. A current density of 1 mA.cm^{-2} is applied for both charge and discharge cycles in order to observe the cycling performance of the electrodes for 3000 cycles, results of which are provided in Figure 2.10. Coulombic efficiencies of the fabricated thin film electrodes are also plotted within the same figure. A high capacity retention of 80% is obtained after 3000 cycles. A coulombic efficiency of more than 95% indicated the

supercapacitive behavior throughout the GCD cycles. It is also noteworthy that the initial drop in capacity is more drastic in the first 1500 cycles, while the Co_3O_4/SWNT nanocomposite electrodes sustained their charge storage performance in the subsequent charge discharge cycles. For further clarification of the observed capacity drop, detailed microstructural analysis is performed via TEM analysis on the samples that are prepared and galvanostatically charged and discharged for 1500 and 3000 cycles. Related TEM images for these samples with their selected area diffraction (SAED) patterns are provided in Figure 2.10. Micrographs at different magnifications for these samples are provided in Figure 2.2 for the prepared and 1500 and 3000 times cycled electrodes. Nanoflake morphology is evident from the low resolution TEM images, where nanocrystalline domains with an average crystallite size of 10 nm become visible in high resolution images. From the SAED patterns for both 1500 and 3000 times cycled electrodes, d–spacing values and the corresponding diffraction planes were identified and were listed in Table 2.1. It is clear that the electrodes are not experiencing a major structural change upon cycling due to the intercalation/deintercalation of Li^+ ions, which can be inferred both from the micrographs and the resulting d-spacing values. Thus, the decrease in cyclic performance for the first 1500 cycles is not due to the morphological changes of the electrodes. It is highly probable that the drop in capacitance can be through aging of the nanocomposite electrodes due to the use of an organic electrolyte in ambient conditions [121].

Results obtained from literature regarding cobalt oxide based supercapacitor electrodes are correlated and can be seen in Table 2.2. While our findings are comparable to some of those in literature, this work shows the ease of fabrication of low cost Co_3O_4/SWNT nanocomposites, which can be operated at wider potential windows in anodic region with organic electrolytes showing promising electrochemical performance.
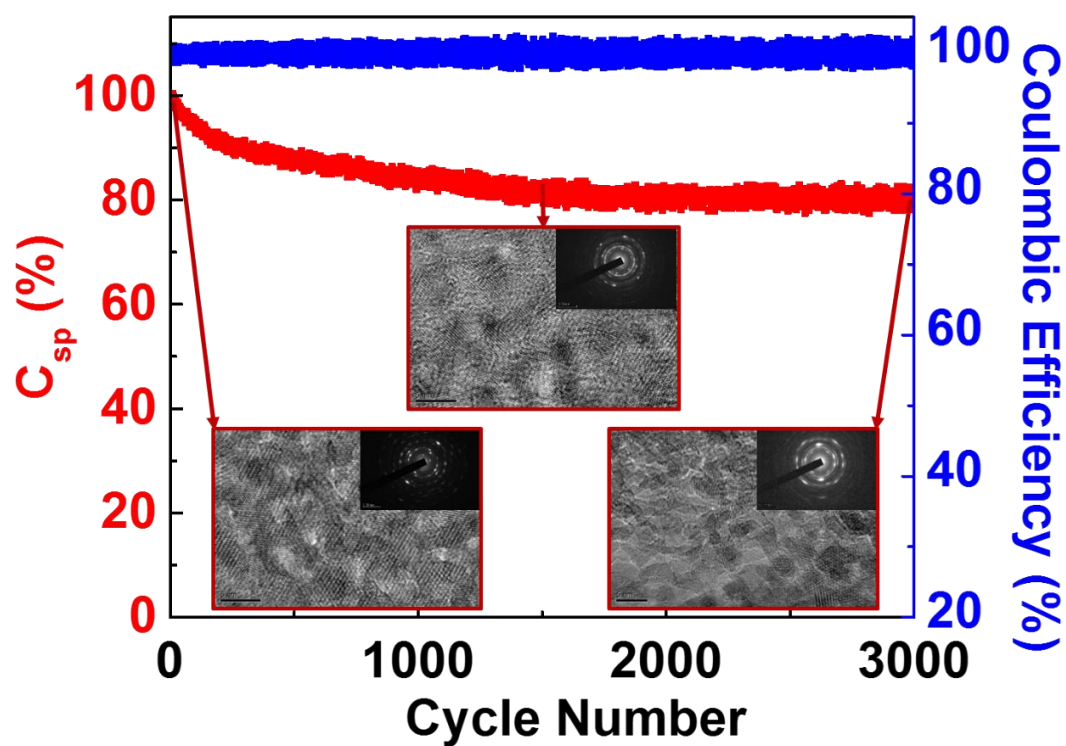
Figure 2.10 Capacity retention and coulombic efficiency of of Co_3O_4/SWNT nanocomposite electrodes at current density of 1 $mA.cm^{-2}$ for 3000 cycles and respective TEM images of as prepared Co_3O_4/SWNT nanocomposite films after 1500 and 3000 cycles [115].

Table 2.2 Parameters of cobalt oxide based supercapacitors from literature (SCE: saturated calomel electrode, ITO: Indium tin oxide, PANI: polyaniline, PET: Polyethylene terephthalate) [115].

Electrode Material	Electrolyte	Voltage or Potential Window	Current Density or Scan Rate	Capacitance	Reference
Co_3O_4 thin film on stainless steel substrate	1 M KOH	-0.2 to 0.5 V (vs. SCE)	5 mV/s	363 F/g	[94]
Co_3O_4 nanowires on nickel foam	6 M KOH	-0.4 to 0.6 V (vs. SCE)	5 mA/cm^2	746 F/g	[75]
Co_3O_4 thin film on stainless steel substrate	1 M KOH	-0.1 to 0.55 V (vs. Ag/AgCl)	2 A/g	454.7 F/g	[96]
Graphene nanosheet/Co_3O_4	6 M KOH	0 to 0.4 V (vs. SCE)	10 mV/s	243.2 F/g	[102]
Co_3O_4 nanobeads-CNTs-graphene nanosheets on nickel foam	7.5 M KOH	0 to 1.2 V	0.7 A/g	600.19 F/g	[39]
Co_3O_4/$Co(OH)_2$ on copper foils	1 M KOH	-0.1 to 0.5 V (vs Ag/AgCl)	2 mV/s	601 mF/cm^2	[97]
Mesoporous Co_3O_4 on nickel foam	1 M KOH	0 to 0.6 V (vs. Ag/AgCl)	1 A/g	880 F/g	[76]
Ultrafine Co_3O_4 nanocrystals on PET/ITO	H_3PO_4/PVA	-0.35 to 0.35 V	0.9 A/g	172 F/g	[104]
Co_3O_4/SWNT thin film	1 M LiClO$_4$ in PC	0 to 1.2 V (vs. Ag/AgCl)	1 mV/s	313.9 F/g	This work

2.4   Conclusions

To conclude, Co_3O_4/SWNT nanocomposite were fabricated with a simple and cost-effective solution based route. Pseudocapacitive Co_3O_4 nanoflakes were successfully deposited on the SWNT thin films which are the only current collectors. Co_3O_4/SWNT nanocomposite electrodes are fabricated and proved to be promising for anodic electrodes for electrochemical storage systems. A specific capacitance of 313.9 F/g at a scan rate of 1 mV/s is obtained, where a capacity retention up to 80% was attained after 3000 charge-discharge cycles. The use of electrodeposition method for the deposition of Co_3O_4 nanoflakes onto SWNT thin films provided a 3-dimensional and porous structure, which is advantageous for electrochemical supercapacitors. While many different fabrication routes exist, this route enables large-scale fabrication onto different substrates, which can be even flexible or stretchable, and this work can be easily extended to various other metal oxide systems.

CHAPTER 3

MICRO-SUPERCAPACITOR FABRICATION FROM SINGLE-WALLED CARBON NANOTUBE BUCKYPAPERS BY LASER ABLATION

3.1   Introduction

The requirement for micropower sources and small-scale energy storage units increases in tandem with the technological trend towards miniaturized and power hungry electronic devices. While small batteries exists for current technology in microelectromechanical systems, personal and military wearable technology and biosensors, their short lifetime and limited power densities hinder further improvements in aforementioned systems. Supercapacitors offer high power density in addition to high cycling capability and are offered as a replacement for batteries for miniaturized electronic devices. Provided that the current supercapacitors are miniaturized to micron scale, called as microcapacitors or micro-supercapacitors, they can satisfy micropower demands of the aforementioned devices [122].

There are different designs for micro-supercapacitors that can be related to the device architecture or fabrication route. Thin film microcapacitors are especially preferred due to their scalable fabrication route with relatively low cost. However, fabricating thicker electrodes yield lower specific capacitance due to harder ionic transfer. Thus, microcapacitors are stacked on each other rather than increasing the mass and thickness of the thin film microcapacitor. Fabrication methods such as sputtering [123], chemical vapor deposition [124], inkjet printing [125], electrochemical deposition [126] can be used to obtain thin film electrodes, which can then be patterned to obtain micro-scale supercapacitor devices. Moreover, as in supercapacitors, micro-supercapacitors can be either EDLC type or pseudocapacitive depending on the active material. Typical electrode active materials utilized in micro-supercapacitors include graphene [127], graphite oxide [128], CNTs [129], PANI [130], MnO_2 [131] and $Co(OH)_2$ [132].

In this work, micro-supercapacitors were fabricated via laser ablation of binder-free SWNT buckypapers on glass substrates without any need for interdigitated contacts. SWNT buckypapers acted as the only current collectors. This route offers a low cost and scalable fabrication of microcapacitor devices. Capacitive behaviour of SWNT microcapacitors were investigated through CV, GCD and EIS.

3.2   Literature Review

3.2.1   Design and Fabrication of Micro-supercapacitors

Performance of microcapacitors heavily depend on the design, or "architecture", of the cell on top of the properties of the active materials that are used. Considerations regarding the performance of SCs such as used electrolyte, pore size of electrode material, ionic conductivity and matching ionic size of the electrolyte with porous structure are still important in order to obtain good capacitive properties, yet in micro-scale, architecture of the cell is the deciding factor of resulting capacitance. Architecture of microcapacitors can be divided into two parts, namely thin film microcapacitors with interdigital in-plane architecture and 3D architectures.

3.2.1.1 Interdigital In-plane Architecture

First microcapacitors adopted the idea of thin film SC design, where two thin film electrodes that are generally thinner than 10 µm, seperated with a solid electrolyte and stacked onto each other with current collectors to obtain a SC cell. To obtain a micro-scale device, this 2D desing is altered to fabricate microelectrodes, or fingers, interdigitally arranged on a substrate; hence, the name of the design is interdigital in-plane architecture [122]. Difference between the conventional 2D SC design and interdigital in-plane architecture can be seen in Figure 3.1.
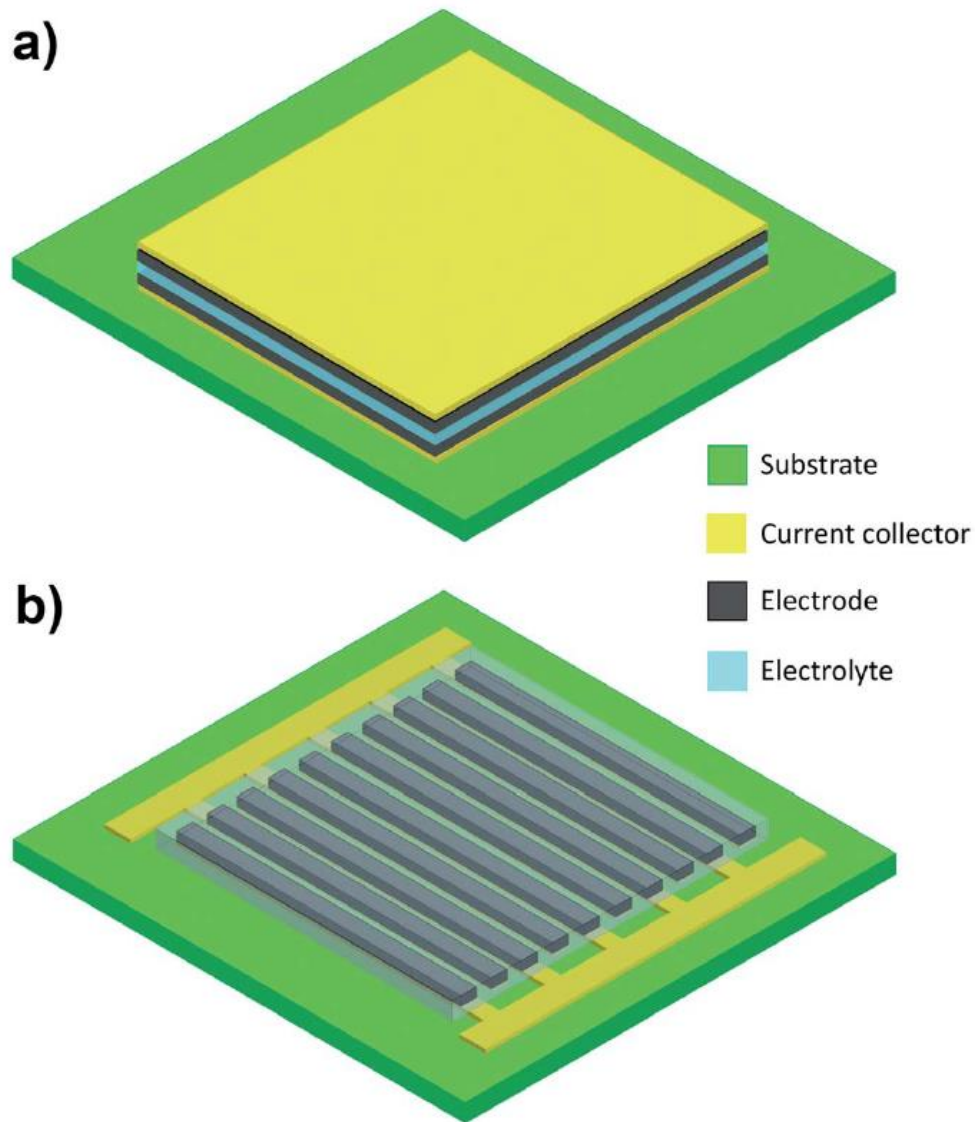
Figure 3.1 Schematics of (a) conventional 2D architecture and (b) interdigital in-plane architecture. Microelectrodes or finger electrodes forms an interdigital in-plane architecture of microcapacitors [122].

This design is especially useful for cost-effective mass production, yet the energy and power density of the cell is limited due to the small footprint of the device. This is because making thicker electrodes is not an option since electron and ion transport is affected adversely. However, it is possible to obtain very small finger spacing (or electrode spacing), decreasing the ion transport resistance. Moreover,

electrode/electrolyte interface also exists at the sides of the finger electrodes, resulting in an increased accessability through the thickness of the thin film. It should be noted that the areal energy density is still limited due to the small footprint area of the device [122].

Pech et al. fabricated micro-supercapacitors through inkjet printing [133]. In this work, activated carbon (AC) ink has been deposited through inkjet printing (75 µm wide 750 µm long and 75 µm of interspace between fingers) onto prepared gold current collectors on oxidized silicon substrate. A representative schematicc and corresponding CV characteristic of the fabricated devices can be seen in Figure 3.2. 1 M Et_4NBF_4 in PC electrolyte was used as the electrolyte and an areal capacitance of 2.1 mFcm^{-2} was obtained at a scan rate of 1 mVs^{-1} [133].
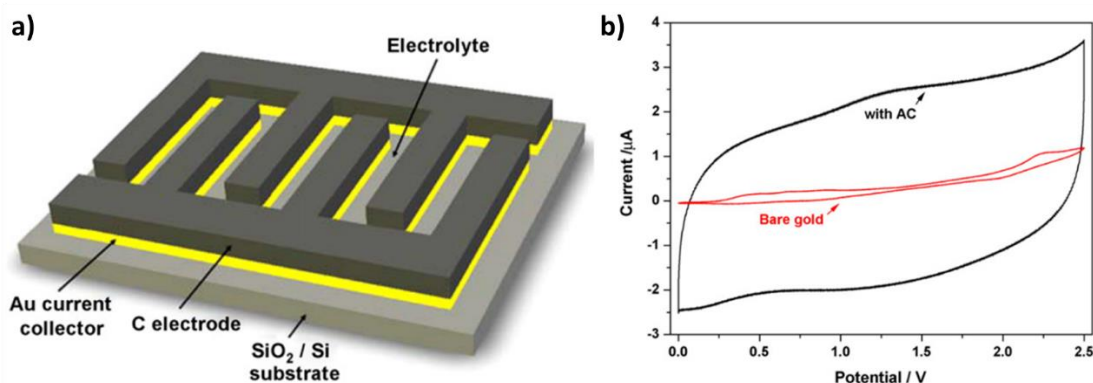
Figure 3.2 (a) Schematic of the fabricated micro-supercapacitor by Pech et al. (b) CV voltammograms of bare gold current collectors and micro-supercapacitor with AC in 1 M Et_4NBF_4 in PC electrolyte at a scan rate of 100 mV^{-1} [133].

El-Kady and Kaner [127] reported direct fabrication of interdigitated micro-supercapacitors with graphene as active material using a DVD burner (Light Scribe). The fabrication route itself offer a cost-effective method with scalability, simply using direct-to-disc labelling technology, which is used to create desired shapes onto the surface of CDs and DVDs. Schematics of the fabrication route can be seen in Figure 3.3. Prepared graphite oxide films were burned using LightScribe DVD with desired

shape to obtain graphene circuits via absorption of high intensity light. This simple scribing method, both reduces the graphite oxide to graphene and patterns the electrodes at the same time. A volumetric capacitance of 2.35 Fcm^{-3} was obtained at a current density of 16.8 $mAcm^{-3}$. Results showed that the utilized fabrication route is promising for the production of micro-supercapacitors [127].
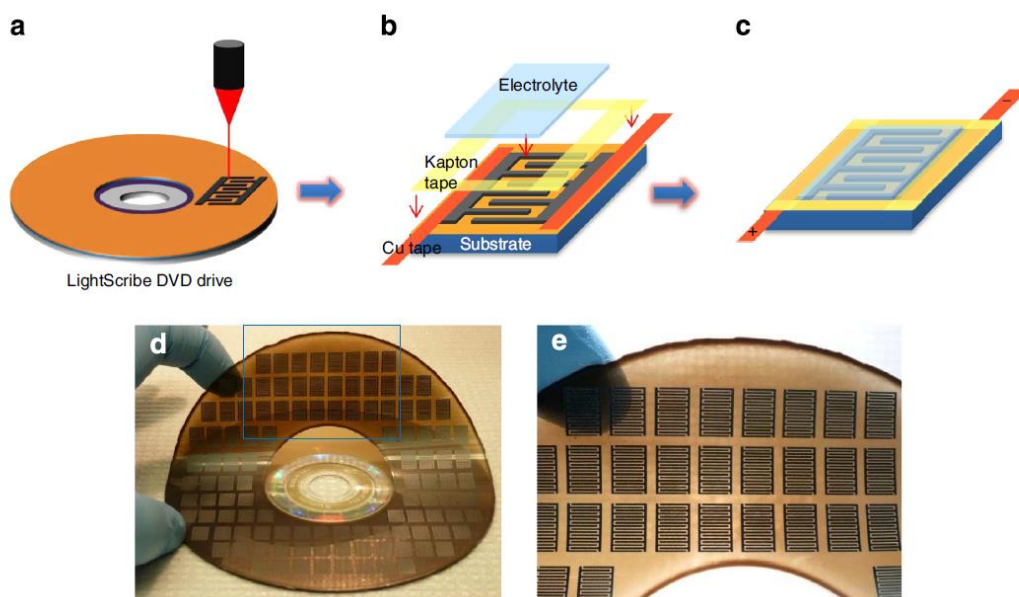
Figure 3.3 (a)-(c) Schematics of the fabrication process of micro-supercapacitors using direct-to-disc labelling technology. PET sheet was used as substrate for graphite oxide that is to be scribed by laser inside the drive. (d), (e) Photos of the fabricated micro-supercapacitors showing the scalability of this method used by El-Kady et al. [127].

In-situ chemical polymerization [130], chemical vapor deposition [131,132], laser reduction of graphite oxide [128,134], electrospinning [135], electrostatic spray deposition followed by photolithography [136] and wet spinning [137] are the other routes that were used to obtain micro-supercapacitors with an interdigital in-plane architecture.

3.2.1.2 Micro-supercapitors with 3D Architecture

Three-dimensional (3D) design for energy storage devices, especially for micro-batteries, are suggested to maximize the energy and power density. 3D matrix of electrodes allows one dimensional (1D) transport between the electrodes, increasing energy density in a small footprint area [138]. Suggested architectures for micro-batteries are schematically shown in Figure 3.4.
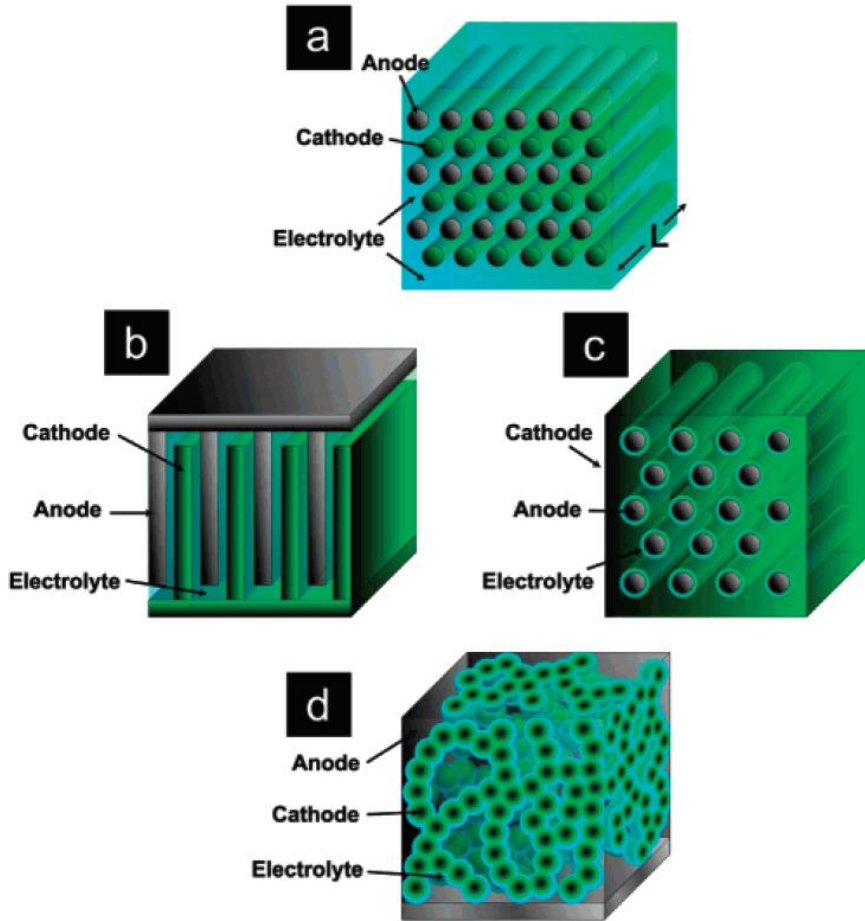
Figure 3.4 Schematics suggested 3D architectures of micro-batteries (a) Cylindrical cathodes and anodes in arrays. (b) Array of cathodes and anodes on interdigitated plates. (c) Cylindrical anodes coated with thin layer of electrolyte and cathode material as the matrix. (d) Sponge like solid network coated with a thin layer of electrolyte as cathode and remaining matrix as the anode material [138].

Similar architectures to those in Figure 3.4 can also be suggested for the fabrication of 3D micro-supercapacitors. As in micro-batteries, biggest advantage of 3D architecture would be the decrease of electrolyte ion path in micro-supercapacitors. Since SC materials are more conductive than battery materials, adopting 3D structure for micro-supercapacitors is more viable than for micro-batteries [122].

3D architecture for micro-supercapacitors has also been investigated by Beidaghi et al. [139] where carbon microelectromechanical systems technique (C-MEMS) was used to fabricate interdigitated carbon micro-electrode arrays (Figure 3.5). Desired architecture was fabricated using C-MEMS to obtain glassy carbon structures and then pyrolyzed and converted into carbon. Prepared carbon micro-structure was electrochemically activated to enhance its capacitive behavior. A specific capacitance 75 mFcm^{-2} was obtained for the fabricated micro-supercapacitors at a scan rate of 5 mV/s [139].
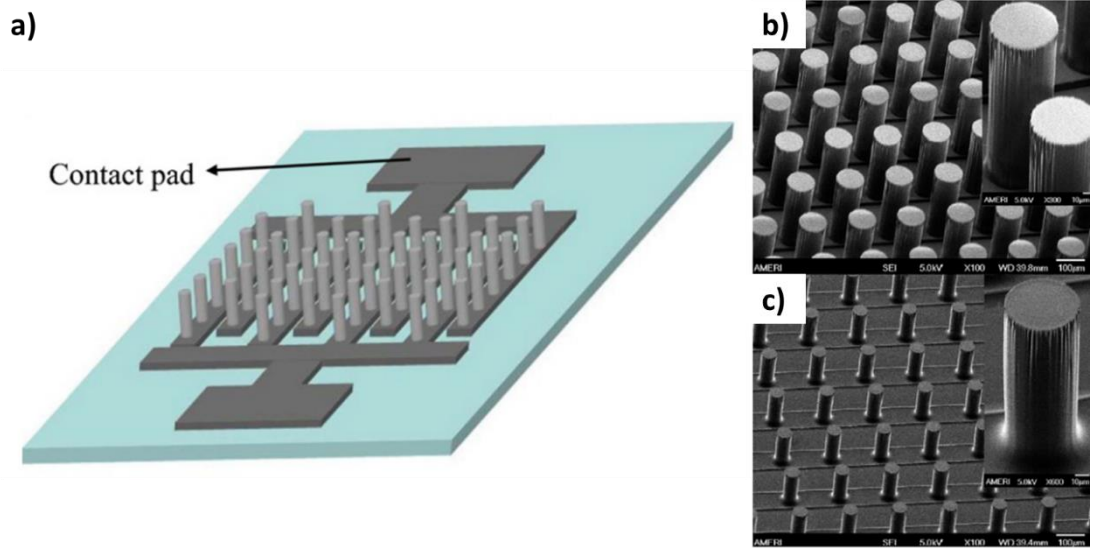
Figure 3.5 (a) A schematic of the 3D architecture after carbonization. SEM images of b) photoresist material and (c) carbonized structure [139].

Shen et al. [140] used inductively coupled plasma technique to obtain 3D interdigitated channels, which were then insulated via deposition of silica (SiO_2) using plasma enhanced chemical vapor deposition. This method was followed by the evaporation of Ti/Au as the current collector layer. Afterwards, slurry of activated carbon formed with polyvinylidene fluoride (PVDF) and N-methyl-2-pyrrolidone (NMP) was injected to the channels and solidified to obtain a self supporting micro-supercapacitor. Photos of fabricated micro-supercapacitor in different stages of fabrication are provided in Figure 3.6. From the fabricated devices a specific capacitance of 98.9 mF.cm^{-2} was obtained at a current density of 16.67 mA.cm^{-2} [140]. Although promising cell performance was obtained, a complicated and costly fabrication process was utilized, which outweigh the advantages.
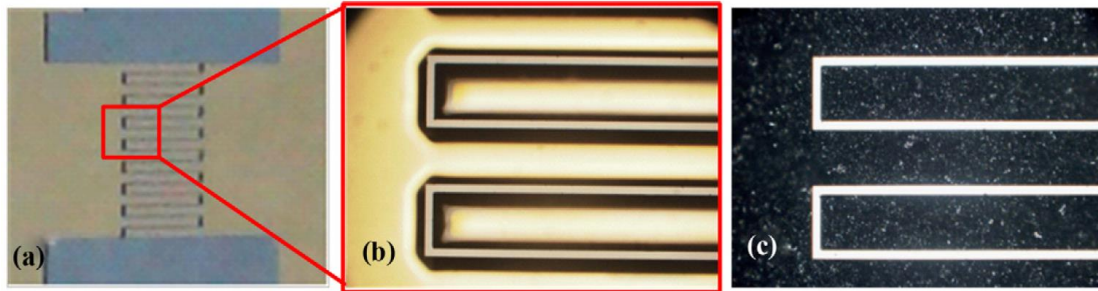
Figure 3.6 (a) and (b) Photos of the interdigitated channels seperated with silicon walls on a gold layer. (c) SEM image of the cell after the injection of composite electrode materials [140].

Apart from the above examples, there are not much different examples of 3D architecture for micro-supercapacitors, and the route for fabrication generally consists of MEMS or C-MEMS routes [141–143]. Still, reported capacitance values for 3D architectures show promising results when their small footprint areas are considered.

3.2.2 Electrochemical Performance Calculations for Micro-Supercapacitors

Gravimetric capacitance in micrometer-thin electrodes is almost negligible when used as micro-supercapacitors. Furthermore, total mass of the cell is generally much higher than the electrode active material, making active material mass negligible [144]. In such cases, Arthur et al. [145] proposed that the footprint area of the device is the most important factor for such miniaturized energy storage devices, making areal energy and power density as the two reliable performance metrics for the characterization of micro-supercapacitors.

Areal capacitance (mF.cm^{-2}) of the cell should be calculated according to the gaps between the electrodes in addition to the area of the finger electrodes. Furthermore, stack capacitance should be calculated taking current collector thickness into account if it exists, and total cell volume should be used for calculations.

Areal capacitance of the cell can be calculated from the CV graphs according to the formula:

$$C_{sp} = \frac{Q}{\Delta E x A}$$

, where Q is the total charge passed (C), ΔE is the voltage window (V), and A is the area of anode and cathode electrodes including the gaps between the finger electrodes (cm^2).

3.3 Experimental Section

3.3.1 Materials

SWNTs used in this study with an approximate diameter and length of 1.8 nm and 5 μm respectively are obtained from TUBALL. Sodium dodecylbenzenesulfonate (SDBS) is obtained from Sigma-Aldrich. PTFE membranes (JMWP04700, 5.0 μm pore size) are purchased from Merck Millipore. All materials are used without further purification.

3.3.2 Preparation of SWNT Buckypapers

SWNT buckypapers on glass substrates are prepared using vacuum filtration method followed by the consecutive transfer of the filtrated buckypaper to glass substrates. For the preparation of the buckypapers, 1 gr SDBS is dissolved in 200 mL of isopropanol using tip sonication for 5 minutes. Afterwards, SWNTs are added (0.5 mg/mL) to the solution and further tip sonication is conducted for annother 5 minutes to obtain a homogenous dispersion. 10 mL of the dispersion is vacuum filtrated onto the filter membrane, which corresponds to 5 mg of SWNTs. After washing several times with isopropanol and DI water, filtrated SWNT film on the filter membrane is transferred onto the glass substrates that are cleaned beforehand via sonication in acetone, isopropanol and DI water for 15 minutes each followed by an oxygen plasma treatment for 5 minutes (Femto Science CUTE). Filter membranes are washed using ethanol and lifted from the glass substrate while they are still wet. Resulting SWNT buckypaper film on glass substrate was dried at 50 ℃ for 1 hour. A photo of the resulting buckypaper is provided in Figure 3.7. Average resistance of the fabricated buckypapers across the diameter is measured as 8 Ω.
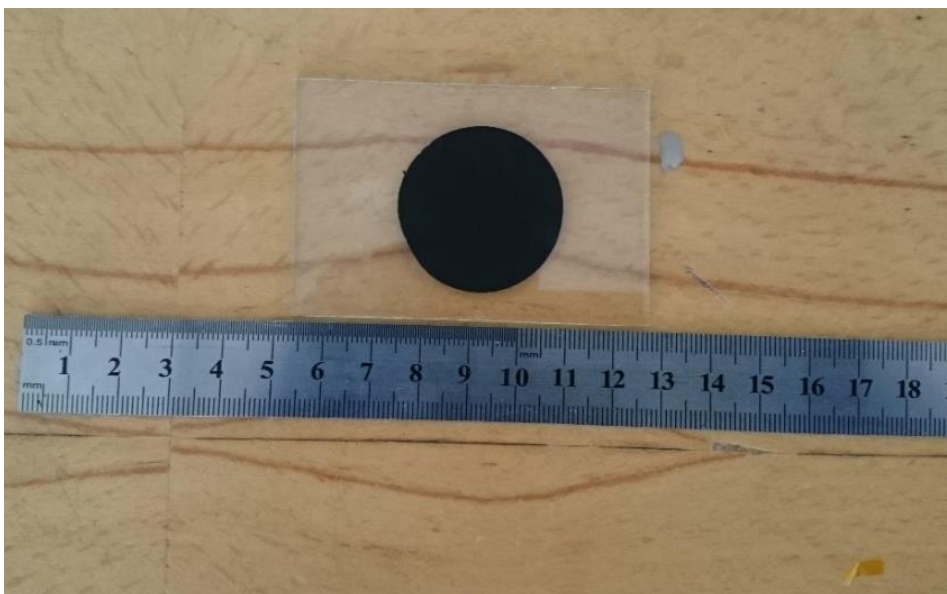
Figure 3.7 A photograph of SWNT buckypaper film on glass substrate.

3.3.3 Fabrication of Buckypaper Micro-Supercapacitor Cell

Two different patterns are fabricated with SWNT buckypapers using EO Technics Laser Marker (50 µm spot size, 1064 nm wavelength, 30W power output at 100% power usage). First patterning is a single line seperating the buckypaper into two electrodes by applying the laser marker at 95% power output at 70 kHz frequency with 10 times sweeping. Second patterning included 24 interdigitated finger electrodes with 12 electrodes for both anode and cathode. Required design is drawn in AutoCAD 2017 software and transferred to the laser marker software. Afterwards, laser marker is applied at a power output of 95% and frequency of 70 kHz with 40 times sweeping. After laser ablation, buckypapers are cleaned with acetone and nitrogen in order to clean the residual carbon on ablated surfaces. Photos of the fabricated micro-supercapacitor electrodes following patterning can be seen in Figure 3.8. Resistance is controlled via contacts that are applied prior to patterning using a multimeter after the ablation to see if anode and cathode is completely seperated. In both samples, the resistance is found to be approximately 250 kΩ following patterning.

3.3.4 Characterization of the Buckypaper Micro-Supercapacitor Cell

In order to obtain precise dimensions of the finger electrodes and the gap created with laser ablation, SEM analysis is conducted. SEM images of the micro-supercapacitors fabricated in this work are provided in Figure 3.9. Gold is sputtered prior to SEM analysis to prevent charging due to the glass substrate. Width of the finger electrodes is measured as 874 ± 1 µm from Figure 3.9 (a). The average width of the gap created by laser ablation is measured as 112 ± 12 µm using Figure 3.9 (b). It is also possible to obtain the length of the finger electrodes by substracting the half of the gap as 2.45 cm. The substracted amount can be ignored sice it is very small compared to the initial design. The morphology of the laser ablated surfaces can be seen from the SEM image provided in Figure 3.9 (c). Figure shows evident damage of SWNTs due to ablation. The thickness of the electrode was measured as 13.5 ± 1.0 µm. from cross-sectional SEM image provided in Figure 3.9 (d).
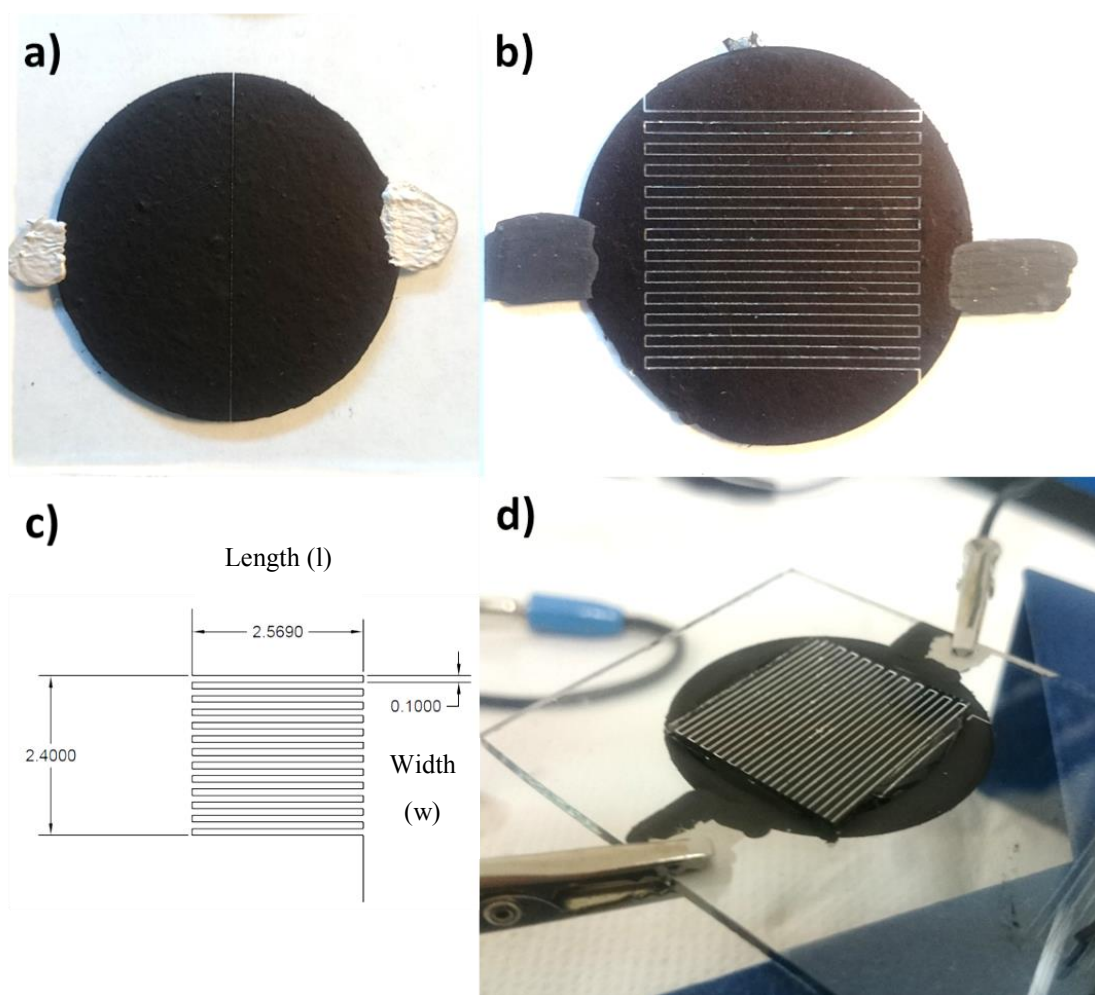
Figure 3.8 Photos of the laser ablated buckypapers with (a) a single line and (b) interdigitated finger electrodes. (c) AutoCAD 2017 was used for patterning. (d) A photograph of the micro-supercapacitor cell prepared with $TBAPF_6$:PMMA:PC:ACN gel electrolyte for electrochemical measurements.
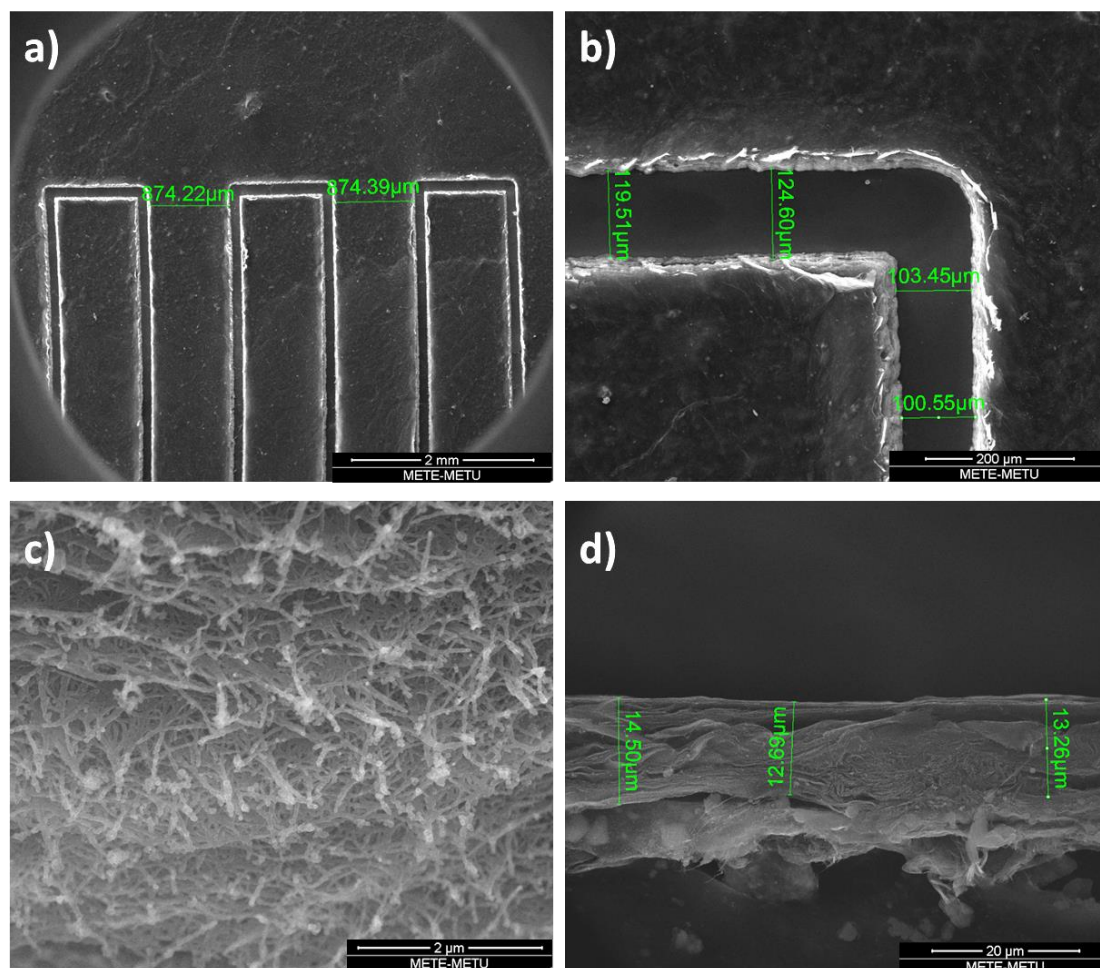
Figure 3.9 SEM images of a micro-supercapacitor fabricated with interdigitated finger electrodes using SWNT buckypapers. SEM image shoowing the (a) width of the electrodes and (b) width of laser ablated surface. (c) High magnification SEM image of laser ablated surface of SWNT buckypaper film. (d) Cross-sectional SEM image of one of the finger electrodes showing the thickness of the buckypaper film.

3.4 Results and Discussion

3.4.1 Electrochemical Characterization

For electrochemical characterizations, $TBAPF_6$:PMMA:PC:ACN gel electrolyte with weight percentages of 3:7:20:70 was prepared and dropwise transferred onto the both single lined and interdigitated finger designed buckypapers dropwise. Then, with the help of a glass slide, gel electrolyte was spread onto the buckypaper in order to fill all of the gaps as shown in Figure 3.8 (d). Electrochemical measurements for both designs were made using CV, GCD and EIS.

Figure 3.10 shows the electrochemical measurements of the single line patterned buckypaper (Figure 3.8 (a)). Electrochemical testing on this sample was actually done in order to perceive the importance of intricate patterns to increase the interaction of electrode/electrolyte interface and decrease the path for the ion conduction. As it can be seen from the CV results (Figure 3.10 (a)), even though the buckypaper formation is preserved, the cell shows resistive behavior. Weak capacitive behavior can be further confirmed through GCD measurements, results of which are provided in Figure 3.10 (b). EIS results also points out that the cell fabricated with single line patterned buckypaper does not have supercapacitive behavior. Capacitance of the cell was found as 2 mF at an applied current of 0.5 mA using cyclic charge discharge as shown in Figure 3.10 (d).

Current values instead of current density is given in both CV and GCD measurements since the effective capacitive area cannot be deduced for the single line patterned buckypaper. Using same current values also made electrochemical comparison of single line patterned buckypaper with buckypaper with interdigidated finger electrodes possible.
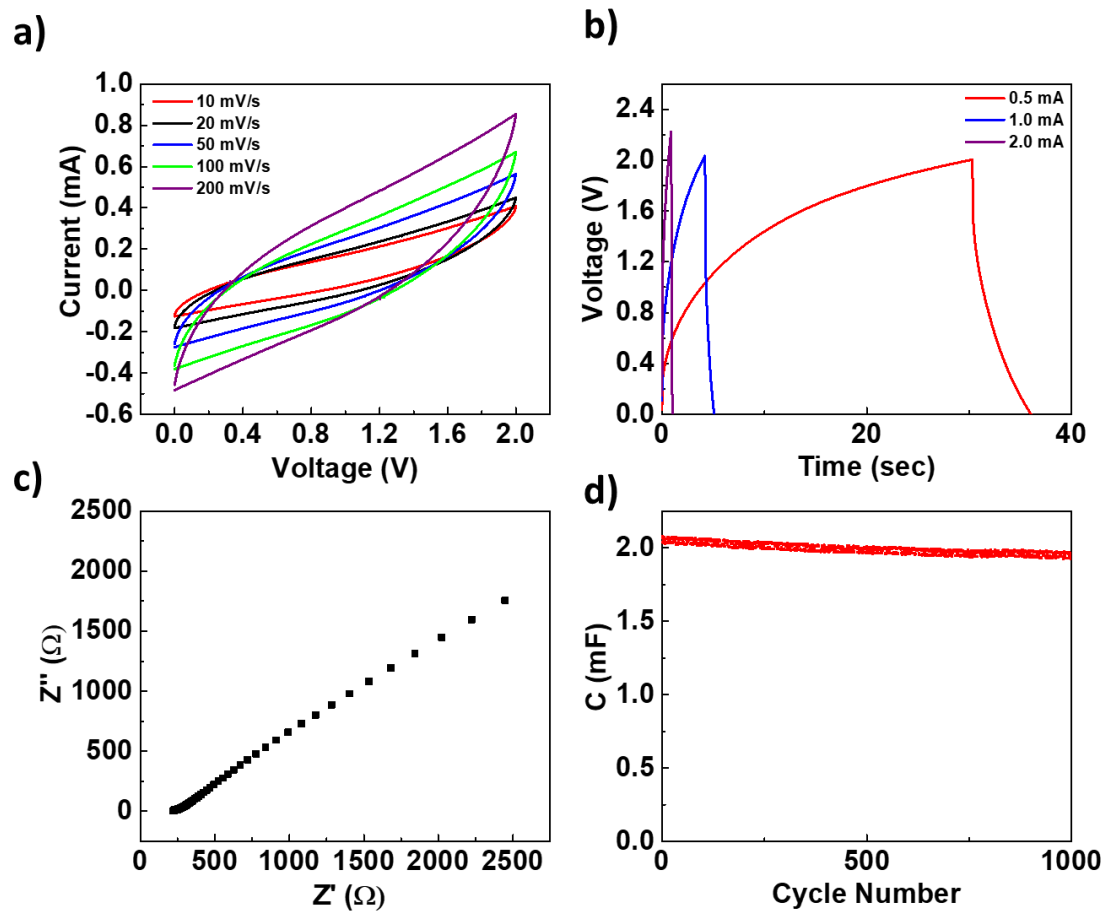
Figure 3.10 Electrochemical measurements for single line patterned buckypaper. (a) CV results with different scan rates, (b) GCD with different currents applied, (c) EIS results between 100 kHz and 0.01 Hz with an AC perturbation of 5 mV and (d) capacity retention during 1000 cycles with an applied current of 0.5 mA.

Figure 3.11 shows the electrochemical measurements of the micro-supercapacitor buckypaper with interdigitated finger electrodes. Unlike the first sample, interdigitated electrode pattern shows behavior close to an ideal supercapacitor. This can be confirmed from CV results provided in Figure 3.11 (a). The fabricated micro-supercapacitor show almost rectangular CV shape at varying scan rates. GCD measurements under applied currents ranging from 0.1 to 2 mA are also conducted and the results are shown in Figure 3.11(b). Coulombic efficiencies were calculated as 83% for 0.1, 0.25 and 0.5 mA currents, 81% for 1 mA and 71 % for 2 mA. Decreased coulombic efficiency upon an increase in the current from 1 to 2 mA is due to an increased IR drop and possibly due to diffusion limitations of the gel electrolyte. Equivalent series resistance of the micro-supercapacitor cell was obtained from impedance spectra (Figure 3.11 (c)) as 118 Ω. High resistance of the fabricated cell is due to the contacts and gel electrolyte in addition to the lack of a separate current collector layer between the electrode material and the substrate. SWNT buckypaper is used as the current collector in this work. It should be noted that the measurements were also made in open atmosphere, where the gel electrolyte is exposed to air. This would possibly result in a decrease in the performance of the cell. Even still, fabricated micro-supercapacitor shows decent supercapacitive behavior at low frequencies unlike the former sample. Moreover, cyclic charge discharge measurements under an applied current of 3 mA is conducted and the results can be seen in Figure 3.11 (d). The capacitance is found as 6.76 mF and dropped only to 6.56 mF after 1000 cycles, showing an excellent capacity retention of 97%.
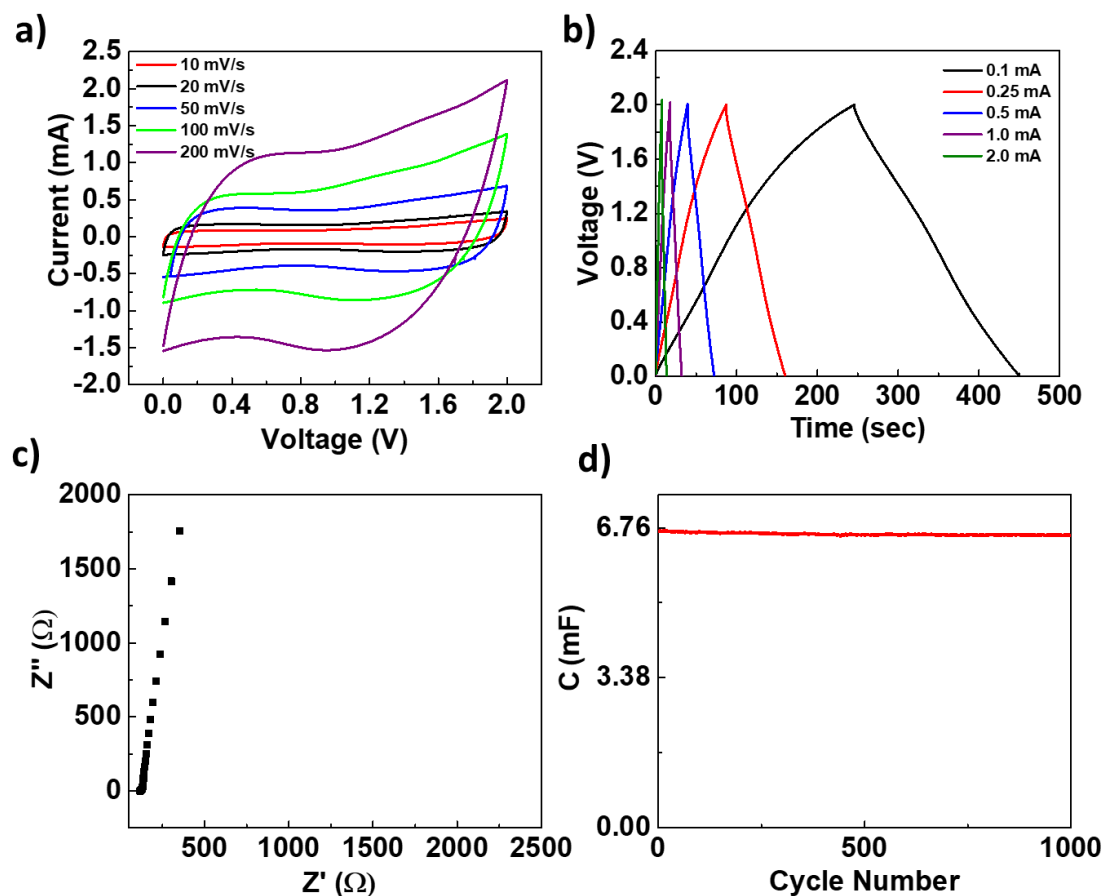
Figure 3.11 Electrochemical measurements for the buckypaper with interdigitated finger electrodes. (a) CV results with different scan rates, (b) GCD with different applied currents, (c) impedance spectroscopy between 100 kHz and 0.01 Hz with 5 mV AC perturbation and (d) charge discharge profile during 1000 cycles with an applied current of 3 mA.

CV results, GCD measurements and impedance spectra of both samples are compared on the same graphs to visualize the importance of design in micro-supercapacitors. These results are provided in Figure 3.12. For all three measurements, it is clear that the buckypaper with interdigitated electrodes yields supercapacitive behavior.
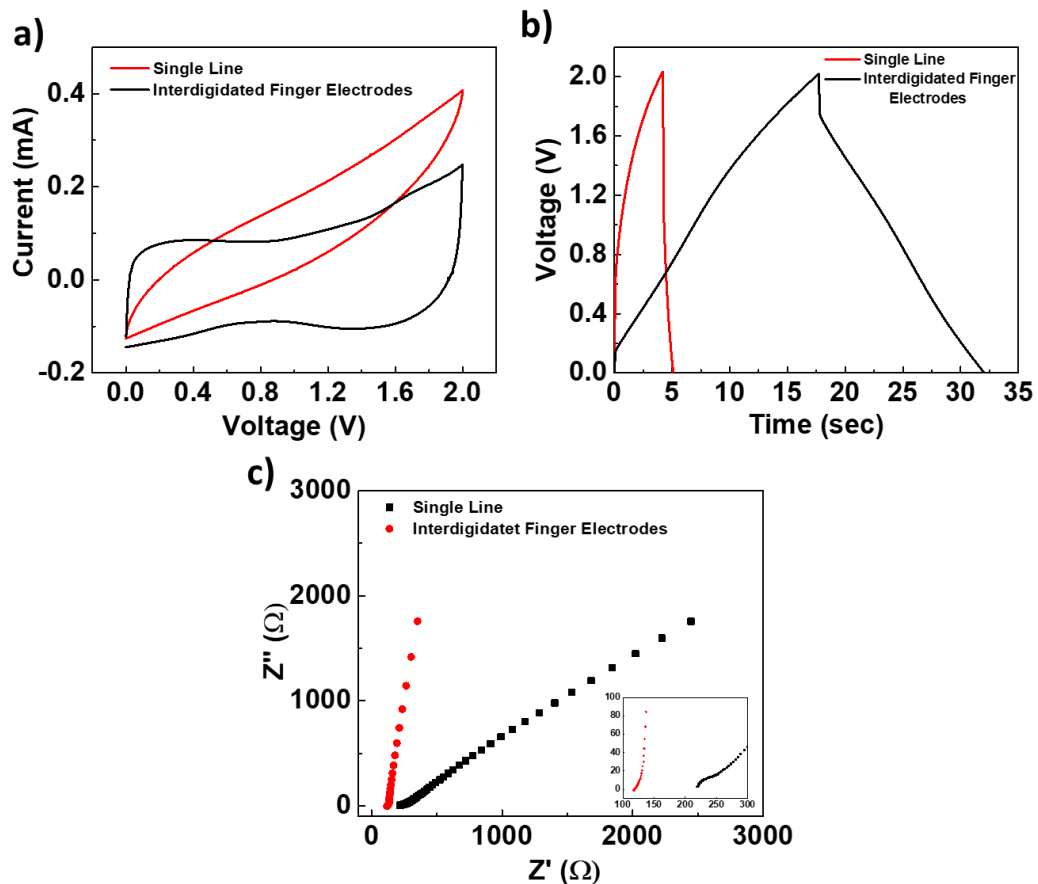
Figure 3.12 Comparison of electrochemical results obtained from buckypaper electrode laser ablated with single line and micro-supercapacitor buckypaper with interdigitated finger electrodes. (a) CV graphs at a scan rate of 10 mV/s, (b) GCD graphs obtained with a current of 1 mA and (c) Comparison of the impedance spectra obtained between 100 kHz to 0.01 Hz frequency with an AC perturation of 5 mV.

Performance of the buckypaper with interdigitated finger electrodes is also calculated as described in Chapter 3.2.2. The effective area of the micro-supercapacitor is calculated from the dimensions obtained from SEM images (Figure 3.9) for 24 electrodes in total and found to be 5.92 cm^2. From the CV measurement in Figure 3.11 (a), specific capacitance of the fabricated cell is calculated as 3.50, 3.13, 2.69, 2.26 and 1.81 mF.cm^{-2} for the scan rates of 10, 20, 50, 100, and 200 mV/s, respectively. These results are highly comparable with the literature [146,147]. This clearly shows that the simple route investigated herein to fabricate micro-supercapacitors is highly promising for the fabrication of 3D micro-supercapacitors.

3.5   Conclusions

Micro-supercapacitors based on binder-free SWNT buckypapers on glass substrates are fabricated via simple vacuum filtration method followed by laser ablation technique. Electrochemical performane of the fabricated electrodes were evaluated. An areal specific capacitance of 3.50 mF.cm^{-2} at a scan rate of 10 mV/s is obtained. Furthermore, a capacity retention up to 97% is attained at an applied current of 3 mA after 1000 charge-discharge cycles. Preparation of SWNT buckypapers and the use of consecutive laser ablation to obtain micro-supercapacitor devices are offered as a simple and scalable production route resulting in the fabrication of supercapacitors with promising electrochemical performance.

CHAPTER 4

CONCLUSIONS AND FUTURE RECOMMENDATIONS

4.1   Conclusions

In this thesis, SWNT thin films were further modified through both chemical and physical means to obtain SC electrodes. Electrochemical performances of the SWNT based SC electrodes were investigated and significant conclusions were reached.

In Chapter 2, Co_3O_4/SWNT nanocomposite thin film supercapacitor electrodes were fabricated with a simple and cost-effective approach. Vacuum filtration and consecutive stamping method was used to fabricate binder-free SWNT thin films on glass substrates. Then, cobalt hydroxide was electrodeposited onto the surface of the SWNT thin film via CV within a potential window of 0 to -1.2 V using a scan rate of 20 mV/s with varying deposition cycles. Prepared thin films were oxidized at 190 ℃ at open atmosphere to obtain Co_3O_4/SWNT nanocomposite thin films. Annealed supercapacitor electrodes were compared and best electrochemical performance was obtained from the sample with 30 cycles of deposition. Specific capacitance of the nanocomposite thin film electrode was calculated from CV measurements and found as 313.9 F/g at a scan rate of 1 mV/s. Capacity retention of the electrode was also investigated and obtained as to 80% after 3000 charge-discharge cycles. SWNT thin films were used as the current collectors and allowed the deposition of Co_3O_4 in nanoflake morphology via electrodeposition. Hence, SWNT thin films not only enhanced electrical conduction through the system; but also provided a porous 3-dimensional structure within the electrodes.

In Chapter 3, micro-supercapacitors were fabricated utilizing laser ablated SWNT buckypaper thin films. Vacuum filtraton method was used to fabricate binder-free SWNT buckypapers, which were transferred onto glass substrates and dried without a need of adhesive. Prepared SWNT buckypapers were laser ablated in two different ways to observe the difference in electrochemical performance. A specific capacitance

of 3.50 mF.cm^{-2} at a scan rate of 10 mV/s was obtained from the SWNT buckypaper that was laser ablated to form interdigitated finger electrodes. A capacity retention up to 97% was attained at an applied current of 3 mA following 1000 charge-discharge cycles. Investigated fabrication route is highly promising and offer much simpler and scalable route for the fabrication of micro-supercapacitors, compared to those methods in literature.

4.2   Future Recommendations

This thesis offers simple routes to achieve SC electrodes based on SWNT thin films. First part of this work shows how SWNT thin films can be used to fabricate nanocomposite thin film electrodes, while the second part proves that bare SWNT thin film buckypapers can be used to fabricate a micro-supercapacitor cell. In spite of the conclusions attained in both parts, future work may extend the scope of this thesis. Some suggestions for possible research interests are below:

1. SWNT amount on the thin films in Chapter 2 may be increased (which may require different filters or improved vacuum system) in order to improve ESR of the electrode.

2. An electrochemical cell may be formed from the fabricated nanocomposite thin film electrodes in Chapter 2 and tested.

3. Parameters including length, width and number of the interdigitated finger electrodes (obtained by laser ablation of SWNT thin film buckypapers, Chapter 3) may be controlled precisely in order to gain insights into their effect on electrochemical performance of the fabricated micro-supercapacitor cell.

4. As in Chapter 2, SWNT thin film buckypapers fabricated in Chapter 3 may be integrated with pseudocapacitive materials to obtain nanocomposite micro-supercapacitors.

5. As suggested before, glass substrates can be replaced with alternative substrates that offer flexibility or stretchability.

REFERENCES

[1]   F. Beguin, E. Frackowiak, Supercapacitors, WILEY-VCH Verlag GmbH & Co. KGaA, 2013. doi:10.1002/9783527646661.

[2]   A. Yu, Electrochemical supercapacitors for energy storage and delivery fundamentals and applications, 2013. doi:10.1002/9781118991978.hces112.

[3]   H. E. Becker, U.S. Patent 2 800 616, 1957.

[4]   R. Kotz, M. Carlen, Principles and applications of electrochemical capacitors, Electrochim. Acta. 45 (2000) 2483–2498.

[5]   B.E. Conway, Electrochemical supercapacitors scientific fundamentals and technological applications, (1999) 736. doi:10.1007/978-1-4757-3058-6.

[6]   P. Simon, Y. Gogotsi, Materials for electrochemical capacitors, Nat. Mater. 7 (2008) 845–854. doi:10.1038/nmat2297.

[7]   Auto Solutions, (n.d.). http://www.maxwell.com/solutions/transportation/auto (accessed July 9, 2017).

[8]   Case Studies, (n.d.). http://www.maxwell.com/solutions/power-grid/power-grid-case-studies (accessed July 9, 2017).

[9]   Opening Doors to Space, (n.d.). http://www.esa.int/Our_Activities/Telecommunications_Integrated_Applications/Opening_doors_to_space (accessed July 9, 2017).

[10]   Ultracapacitor Overview, (n.d.). http://www.maxwell.com/products/ultracapacitors (accessed July 9, 2017).

[11]   T. Hamilton, Next Stop : Ultracapacitor Buses, (2009). https://www.technologyreview.com/s/415773/next-stop-ultracapacitor-buses/ (accessed July 9, 2017).

[12]   P. Simon, Y. Gogotsi, B. Dunn, Where do batteries end and supercapacitors begin ?, Science (80). 343 (2014) 1210–1211. doi:10.1126/science.1249625.

[13]   G. Salitra, A. Soffer, L. Eliad, Y. Cohen, D. Aurbach, Carbon electrodes for double-layer capacitors I. relations between ion and pore Dimensions, J. Electrochem. Soc. 147 (2000) 2486. doi:10.1149/1.1393557.

[14]   L.L. Zhang, X.S. Zhao, Carbon-based materials as supercapacitor electrodes, Chem. Soc. Rev. 38 (2009) 2520. doi:10.1039/b813846j.

[15]   Helmholtz, Ueber einige Gesetze der Vertheilung elektrischer Ströme in körperlichen Leitern mit Anwendung auf die thierisch-elektrischen Versuche, Ann. Phys. 165 (1853) 211–233. doi:10.1002/andp.18531650603.

[16]   M. Gouy, Sur la constitution de la charge électrique à la surface d'un électrolyte, J. Phys. Théorique Appliquée. 9 (1910) 457–468. doi:10.1051/jphystap:019100090045700.

[17]   D.L. Chapman, A contribution to the theory of electrocapillarity, Philos. Mag. Ser. 6. 25 (1913) 475–481. doi:10.1080/14786440408634187.

[18]   O. Stern, Zur Theorie der Elektrolytischen Doppelschicht, Zeitschrift Fur Elektrochemie. 30 (1924) 508–516. doi:10.1002/bbpc.192400182.

[19]   A.G. Pandolfo, A.F. Hollenkamp, Carbon properties and their role in supercapacitors, J. Power Sources. 157 (2006) 11–27. doi:10.1016/j.jpowsour.2006.02.065.

[20]   Y. Zhu, S. Murali, M.D. Stoller, K.J. Ganesh, W. Cai, P.J. Ferreira, A. Pirkle, R.M. Wallace, K. a Cychosz, M. Thommes, D. Su, E. a Stach, R.S. Ruoff, Carbon-based supercapacitors produced by activation of graphene, Science (80-.). 332 (2011) 1537–1542. doi:10.1126./science.1200770.

[21]   C. Liu, Z. Yu, D. Neff, A. Zhamu, B.Z. Jang, Graphene-based supercapacitor with an ultrahigh energy density, Nano Lett. 10 (2010) 4863–4868. doi:10.1021/nl102661q.

[22]   M. Kim, Y. Kim, K.M. Lee, S.Y. Jeong, E. Lee, S.H. Baeck, S.E. Shim, Electrochemical improvement due to alignment of carbon nanofibers fabricated by electrospinning as an electrode for supercapacitor, Carbon N. Y. 99 (2016) 607–618. doi:10.1016/j.carbon.2015.12.068.

[23]   C. Kim, K.S. Yang, Electrochemical properties of carbon nanofiber web as an electrode for supercapacitor prepared by electrospinning, Appl. Phys. Lett. 83 (2003) 1216–1218. doi:10.1063/1.1599963.

[24] V.T. Le, H. Kim, A. Ghosh, J. Kim, J. Chang, Q.A. Vu, D.T. Pham, J.H. Lee, S.W. Kim, Y.H. Lee, Coaxial fiber supercapacitor using all-carbon material electrodes, ACS Nano. 7 (2013) 5940–5947. doi:10.1021/nn4016345.

[25] R.R. Salunkhe, J. Tang, Y. Kamachi, T. Nakato, J.H. Kim, Y. Yamauchi, Asymmetric Supercapacitors Using 3D Nanoporous Carbon and Cobalt Oxide Electrodes Synthesized from a Single Metal-Organic Framework, ACS Nano. 9 (2015) 6288–6296. doi:10.1021/acsnano.5b01790.

[26] E. Frackowiak, K. Metenier, V. Bertagna, F. Beguin, Supercapacitor electrodes from multiwalled carbon nanotubes, Appl. Phys. Lett. 77 (2000) 2421. doi:10.1063/1.1290146.

[27] Y. Gao, Y.S. Zhou, M. Qian, X.N. He, J. Redepenning, P. Goodman, H.M. Li, L. Jiang, Y.F. Lu, Chemical activation of carbon nano-onions for high-rate supercapacitor electrodes, Carbon N. Y. 51 (2013) 52–58. doi:10.1016/j.carbon.2012.08.009.

[28] M. Zeiger, N. Jäckel, V.N. Mochalin, V. Presser, Review: carbon onions for electrochemical energy storage, J. Mater. Chem. A. 4 (2016) 3172–3196. doi:10.1039/C5TA08295A.

[29] P. Lv, X.-W. Tan, K.-H. Yu, R.-L. Zheng, J.-J. Zheng, W. Wei, Super-elastic graphene/carbon nanotube aerogel: A novel thermal interface material with highly thermal transport properties, Carbon N. Y. 99 (2016) 222–228. doi:10.1016/j.carbon.2015.12.026.

[30] J. Li, X. Wang, J. Li, Q. Huang, X. Wang, S. Gamboa, Q. Huang, S. Gamboa, P.J. Sebastian, P.J. Sebastian, Studies on preparation and performances of carbon aerogel electrodes for the application of supercapacitor, J. Power Sources. 158 (2006) 784. doi:10.1016/j.jpowsour.2005.09.045.

[31] B. Yuan, C. Xu, D. Deng, Y. Xing, L. Liu, H. Pang, D. Zhang, Graphene oxide/nickel oxide modified glassy carbon electrode for supercapacitor and nonenzymatic glucose sensor, Electrochim. Acta. 88 (2013) 708–712. doi:10.1016/j.electacta.2012.10.102.

[32] T. Brousse, D. Belanger, J.W. Long, To be or not to be pseudocapacitive?, J. Electrochem. Soc. 162 (2015) A5185–A5189. doi:10.1149/2.0201505jes.

[33] B.-O. Park, C.. Lokhande, H.-S. Park, K.-D. Jung, O.-S. Joo, Performance of supercapacitor with electrodeposited ruthenium oxide film electrodes—effect of film thickness, J. Power Sources. 134 (2004) 148–152. doi:10.1016/j.jpowsour.2004.02.027.

[34] D. Xuan, W. Chengyang, C. Mingming, J. Yang, W. Jin, Electrochemical performances of nanoparticle Fe_3O_4/activated carbon supercapacitor using KOH electrolyte solution, J. Phys. Chem. C. 113 (2009) 2643–2646. doi:10.1021/jp8088269.

[35] R. Kumar, R.K. Singh, A.R. Vaz, S.A. Moshkalev, Microwave-assisted synthesis and deposition of a thin ZnO layer on microwave-exfoliated graphene: optical and electrochemical evaluations, RSC Adv. 5 (2015) 67988–67995. doi:10.1039/C5RA09936F.

[36] W. Wei, X. Cui, W. Chen, D.G. Ivey, Manganese oxide-based materials as electrochemical supercapacitor electrodes, Chem. Soc. Rev. 40 (2011) 1697–1721. doi:10.1039/C0CS00127A.

[37] L. Yuan, X. Lu, X. Xiao, T. Zhai, J. Dai, F. Zhang, B. Hu, Flexible solid-state supercapacitors based on carbon nanoparticles / MnO_2 nanorods hybrid structure, ACS Nano. 6 (2011) 656–661. doi:10.1021/nn2041279.

[38] T.C. Liu, W.G. Pell, B.E. Conway, Stages in the development of thick cobalt oxide films exhibiting reversible redox behavior and pseudocapacitance, Electrochim. Acta. 44 (1999) 2829–2842. doi:10.1016/S0013-4686(99)00002-X.

[39] R. Kumar, R.K. Singh, P.K. Dubey, D.P. Singh, R.M. Yadav, Self-assembled hierarchical formation of conjugated 3D cobalt oxide nanobead-CNT-graphene nanostructure using microwaves for high-performance supercapacitor Electrode, ACS Appl. Mater. Interfaces. 7 (2015) 15042–15251. doi:10.1021/acsami.5b04336.

[40] R. Kumar, R.K. Singh, R. Savu, P.K. Dubey, P. Kumar, S.A. Moshkalev, Microwave-assisted synthesis of void-induced graphene-wrapped nickel oxide hybrids for supercapacitor applications, RSC Adv. 6 (2016) 26612–26620. doi:10.1039/c6ra00426a.

[41] G.A. Snook, P. Kao, A.S. Best, Conducting-polymer-based supercapacitor devices and electrodes, J. Power Sources. 196 (2011) 1–12. doi:10.1016/j.jpowsour.2010.06.084.

[42] V. Augustyn, P. Simon, B. Dunn, Pseudocapacitive oxide materials for high-rate electrochemical energy storage, Energy Environ. Sci. 7 (2014) 1597. doi:10.1039/c3ee44164d.

[43] G. Wang, L. Zhang, J. Zhang, A review of electrode materials for electrochemical supercapacitors, Chem. Soc. Rev. 41 (2012) 797–828. doi:10.1039/C1CS15060J.

[44] Y. Huang, M. Zhu, Z. Pei, Q. Xue, Y. Huang, C. Zhi, A shape memory supercapacitor and its application in smart energy storage textiles, J. Mater. Chem. A. 4 (2016) 1290–1297. doi:10.1039/C5TA09473A.

[45] L. Zhan, H. Chen, J. Fang, S. Wang, L.X. Ding, Z. Li, P.J. Ashman, H. Wang, Coaxial Co_3O_4@polypyrrole core-shell nanowire arrays for high performance lithium ion batteries, Electrochim. Acta. 209 (2016) 192–200. doi:10.1016/j.electacta.2016.05.059.

[46] P. Xiong, H. Huang, X. Wang, Design and synthesis of ternary cobalt ferrite/graphene/polyaniline hierarchical nanocomposites for high-performance supercapacitors, J. Power Sources. 245 (2014) 937–946. doi:10.1016/j.jpowsour.2013.07.064.

[47] Y. Liu, Z. Liu, N. Lu, E. Preiss, S. Poyraz, M.J. Kim, X. Zhang, Facile synthesis of polypyrrole coated copper nanowires: a new concept to engineered core–shell structures, Chem. Commun. 48 (2012) 2621. doi:10.1039/c2cc16961d.

[48] P. Bober, J. Stejskal, M. Trchová, J. Hromádková, J. Prokeš, Polyaniline-coated silver nanowires, React. Funct. Polym. 70 (2010) 656–662. doi:10.1016/j.reactfunctpolym.2010.05.009.

[49] Y. Zhang, L. Si, B. Zhou, B. Zhao, Y. Zhu, L. Zhu, X. Jiang, Synthesis of novel graphene oxide/pristine graphene/polyaniline ternary composites and application to supercapacitor, Chem. Eng. J. 288 (2016) 689–700. doi:10.1016/j.cej.2015.12.058.

[50] Z.A. Yu, C. Li, D. Abbitt, J. Thomas, Flexible, sandwich-like Ag-nanowire/PEDOT:PSS-nanopillar/MnO$_2$ high performance supercapacitors, J. Mater. Chem. A. 2 (2014) 10923–10929. doi:10.1039/c4ta01245c.

[51] C. Peng, S. Zhang, D. Jewell, G.Z. Chen, Carbon nanotube and conducting polymer composites for supercapacitors, Prog. Nat. Sci. 18 (2008) 777–788. doi:10.1016/j.pnsc.2008.03.002.

[52] Q. Cheng, J. Tang, J. Ma, H. Zhang, N. Shinya, L. Qin, Polyaniline-coated electro-etched carbon fiber cloth electrodes for supercapacitors, (2011) 23584–23590.

[53] K. Wang, H. Wu, Y. Meng, Z. Wei, Conducting polymer nanowire arrays for high performance supercapacitors, Small. 10 (2014) 14–31. doi:10.1002/smll.201301991.

[54] D.P. Dubal, S. V. Patil, G.S. Gund, C.D. Lokhande, Polyaniline-polypyrrole nanograined composite via electrostatic adsorption for high performance electrochemical supercapacitors, J. Alloys Compd. 552 (2013) 240–247. doi:10.1016/j.jallcom.2012.10.031.

[55] E. Frackowiak, F. Béguin, Carbon materials for the electrochemical storage of energy in capacitors, Carbon N. Y. 39 (2001) 937–950. doi:10.1016/S0008-6223(00)00183-4.

[56] H. Shi, Activated carbons and double layer capacitance, Electrochim. Acta. 41 (1996) 1633–1639. doi:10.1016/0013-4686(95)00416-5.

[57] H. Pan, J. Li, Y.P. Feng, Carbon nanotubes for supercapacitor, Nanoscale Res. Lett. 5 (2010) 654–668. doi:10.1007/s11671-009-9508-2.

[58] E. Frackowiak, V. Khomenko, K. Jurewicz, K. Lota, F. Béguin, Supercapacitors based on conducting polymers/nanotubes composites, J. Power Sources. 153 (2006) 413–418. doi:10.1016/j.jpowsour.2005.05.030.

[59] E. Frackowiak, K. Metenier, V. Bertagna, F. Beguin, Supercapacitor electrodes from multiwalled carbon nanotubes, Appl. Phys. Lett. 77 (2000) 2421–2423. doi:10.1063/1.1290146.

[60] R. Baughman, A. Zakhidov, W. de Heer, Carbon nanotubes the route toward applications, Science (80). 297 (2002) 787–792. doi:10.1126/science.1060928.

[61] W. Dmowski, T. Egami, K.E. Swider-Lyons, C.T. Love, D.R. Rolison, Local atomic structure and conduction mechanism of nanocrystalline hydrous RuO_2 from x-ray scattering, J. Phys. Chem. B. 106 (2002) 12677–12683. doi:10.1021/jp026228l.

[62] G. Wang, L. Zhang, J. Zhang, A review of electrode materials for electrochemical supercapacitors, Chem. Soc. Rev. 41 (2012) 797. doi:10.1039/c1cs15060j.

[63] R. Fu, Z. Ma, J.P. Zheng, Proton NMR and dynamic studies of hydrous ruthenium oxide, J. Phys. Chem. B. 106 (2002) 3592–3596. doi:10.1021/jp013860q.

[64] H.Y. Lee, J.B. Goodenough, Supercapacitor behavior with KCl electrolyte, J. Solid State Chem. 144 (1999) 220–223. doi:http://dx.doi.org/10.1006/jssc.1998.8128.

[65] A. González, E. Goikolea, J.A. Barrena, R. Mysyk, Review on supercapacitors: technologies and materials, Renew. Sustain. Energy Rev. 58 (2016) 1189–1206. doi:10.1016/j.rser.2015.12.249.

[66] J. Tizfahm, M. Aghazadeh, M.G. Maragheh, M.R. Ganjali, P. Norouzi, F. Faridbod, Electrochemical preparation and evaluation of the supercapacitive performance of MnO_2 nanoworms, Mater. Lett. 167 (2016) 153–156. doi:10.1016/j.matlet.2015.12.158.

[67] M. Aghazadeh, M. Asadi, M.G. Maragheh, M.R. Ganjali, P. Norouzi, F. Faridbod, Facile preparation of MnO_2 nanorods and evaluation of their supercapacitive characteristics, Appl. Surf. Sci. 364 (2016) 726–731. doi:10.1016/j.apsusc.2015.12.227.

[68] Z. Liu, K. Xu, H. Sun, S. Yin, One-step synthesis of single-layer MnO_2 nanosheets with multi-role sodium dodecyl sulfate for high-performance pseudocapacitors, Small. 11 (2015) 2182–2191. doi:10.1002/smll.201402222.

[69] G. Lee, Y. Cheng, C. V Varanasi, J. Liu, Influence of the nickel oxide nanostructure morphology on the effectiveness of reduced graphene oxide coating in supercapacitor electrodes, J. Phys. Chem. C. (2014) 2281–2286.

[70] V. Gupta, T. Kawaguchi, N. Miura, Synthesis and electrochemical behavior of nanostructured cauliflower-shape Co-Ni/Co-Ni oxides composites, Mater. Res. Bull. 44 (2009) 202–206. doi:10.1016/j.materresbull.2008.04.020.

[71] A.K. Singh, D. Sarkar, K. Karmakar, K. Mandal, G.G. Khan, High-performance supercapacitor electrode based on cobalt oxide-manganese dioxide-nickel oxide ternary 1D hybrid nanotubes, ACS Appl. Mater. Interfaces. 8 (2016) 20786–20792. doi:10.1021/acsami.6b05933.

[72] C.D. Lokhande, D.P. Dubal, O.S. Joo, Metal oxide thin film based supercapacitors, Curr. Appl. Phys. 11 (2011) 255–270. doi:10.1016/j.cap.2010.12.001.

[73] J. Chen, X. Wu, A. Selloni, Electronic structure and bonding properties of cobalt oxide in the spinel structure, Phys. Rev. B. 83 (2011) 245204–12. doi:10.1103/PhysRevB.83.245204.

[74] Z. Wu, W. Ren, L. Wen, L. Gao, J. Zhao, Z. Chen, G. Zhou, F. Li, H. Cheng, Graphene anchored with Co_3O_4 nanoparticles as anode of lithium ion capacity and cyclic performance, ACS Nano. 4 (2010) 3187–3194. doi:10.1021/nn100740x.

[75] Y. Gao, S. Chen, D. Cao, G. Wang, J. Yin, Electrochemical capacitance of Co_3O_4 nanowire arrays supported on nickel foam, J. Power Sources. 195 (2010) 1757–1760. doi:10.1016/j.jpowsour.2009.09.048.

[76] X. Hu, H. Huang, J. Zhang, J. Shi, S. Zhu, N. Su, Controllable hydrothermal-assisted synthesis of mesoporous Co_3O_4 nanosheets, RSC Adv. 5 (2015) 99899–99906. doi:10.1039/C5RA19789A.

[77] C. Zhong, Y. Deng, W. Hu, J. Qiao, L. Zhang, J. Zhang, A review of electrolyte materials and compositions for electrochemical supercapacitors, Chem. Soc. Rev. 44 (2015) 7484–7539. doi:10.1039/C5CS00303B.

[78] a. Brandt, S. Pohlmann, A. Varzi, A. Balducci, S. Passerini, Ionic liquids in supercapacitors, MRS Bull. 38 (2013) 554–559. doi:10.1557/mrs.2013.151.

[79] B. Akinwolemiwa, C. Peng, G.Z. Chen, Redox electrolytes in supercapacitors, J. Electrochem. Soc. 162 (2015) A5054–A5059. doi:10.1149/2.0111505jes.

[80] V. Khomenko, E. Frackowiak, F. Béguin, Determination of the specific capacitance of conducting polymer/nanotubes composite electrodes using different cell configurations, Electrochim. Acta. 50 (2005) 2499–2506. doi:10.1016/j.electacta.2004.10.078.

[81] S. Ban, J. Zhang, L. Zhang, K. Tsay, D. Song, X. Zou, Charging and discharging electrochemical supercapacitors in the presence of both parallel leakage process and electrochemical decomposition of solvent, Electrochim. Acta. 90 (2013) 542–549. doi:10.1016/j.electacta.2012.12.056.

[82] R. Yüksel, Development of supercapacitors with one dimensional nanomaterials, Middle East Technical University, 2017.

[83] M.D. Stoller, R.S. Ruoff, Best practice methods for determining an electrode material's performance for ultracapacitors, Energy Environ. Sci. 3 (2010) 1294–1301. doi:10.1039/c0ee00074d.

[84] Q. Zhuang, X. Qiu, S. Xu, Diagnosis of electrochemical impedance spectroscopy in lithium-ion batteries, Lithium Ion Batter. – New Dev. (2012) 189–226. doi:10.5772/26749.

[85] D.D. MacDonald, Reflections on the history of electrochemical impedance spectroscopy, Electrochim. Acta. 51 (2006) 1376–1388. doi:10.1016/j.electacta.2005.02.107.

[86] E. Barsoukov, J.R. Macdonald, Impedance Spectroscopy, 2005. doi:10.1002/0471716243.

[87] M. Meyyappan, Nanostructured materials for supercapacitors, J. Vac. Sci. Technol. A. 31 (2013) 508031–14. doi:10.1116/1.4802772.

[88] Z.A. Hu, Y.-X. Wang, Y.-L. Xie, Y.-Y. Yang, Z.-Y. Zhang, H.-Y. Wu, Ag nanowires and its application as electrode materials in electrochemical capacitor, J. Appl. Electrochem. 40 (2010) 341–344. doi:10.1007/s10800-009-0002-4.

[89] R. Yuksel, S. Coskun, H.E. Unalan, Coaxial silver nanowire network core molybdenum oxide shell supercapacitor electrodes, Electrochim. Acta. 193 (2016) 39–44. doi:10.1016/j.electacta.2016.02.033.

[90] B.G. Armstrong, A.R. Armstrong, P.G. Bruce, P. Reale, B. Scrosati, $TiO_2(B)$ nanowires as an improved anode material for lithium-ion batteries containing $LiFePO_4$ or $LiNi_{0.5}Mn_{1.5}O_4$ cathodes and a polymer electrolyte, Adv. Mater. 2 (2006) 2597–2600. doi:10.1002/adma.200601232.

[91] K. Rajendra, N. Miura, Potentiodynamically deposited nanostructured manganese dioxide as electrode material for electrochemical redox supercapacitors, J. Power Sources. 135 (2004) 354–360. doi:10.1016/j.jpowsour.2004.04.005.

[92] C. Hu, K. Chang, M. Lin, Y. Wu, Design and tailoring of the nanotubular arrayed architecture of hydrous RuO_2 for next generation supercapacitors, Nano Lett. 6 (2006) 2690–2695.

[93] J.P. Zheng, T.R. Jow, High energy and high power density electrochemical capacitors, J. Power Sources. 62 (1996) 155–159. doi:10.1016/S0378-7753(96)02424-X.

[94] A.D. Jagadale, V.S. Kumbhar, C.D. Lokhande, Supercapacitive activities of potentiodynamically deposited nanoflakes of cobalt oxide (Co_3O_4) thin film electrode, J. Colloid Interface Sci. 406 (2013) 225–230. doi:10.1016/j.jcis.2013.05.037.

[95] A.D. Jagadale, V.S. Kumbhar, R.N. Bulakhe, C.D. Lokhande, Influence of electrodeposition modes on the supercapacitive performance of Co_3O_4 electrodes, Energy. 64 (2014) 234–241. doi:10.1016/j.energy.2013.10.016.

[96] M. Aghazadeh, M. Hosseinifard, B. Sabour, S. Dalvand, Pulse electrochemical synthesis of capsule-like nanostructures of Co_3O4 and investigation of their capacitive performance, Appl. Surf. Sci. 287 (2013) 187–194. doi:10.1016/j.apsusc.2013.09.114.

[97] M. Qorbani, N. Naseri, A.Z. Moshfegh, Hierarchical $Co_3O_4/Co(OH)_2$ nanoflakes as a supercapacitor electrode: Experimental and semi-empirical model, ACS Appl. Mater. Interfaces. 7 (2015) 11172–11179. doi:10.1021/acsami.5b00806.

[98] S.G. Kandalkar, D.S. Dhawale, C.-K. Kim, C.D. Lokhande, Chemical synthesis of cobalt oxide thin film electrode for supercapacitor application, Synth. Met. 160 (2010) 1299–1302. doi:10.1016/j.synthmet.2010.04.003.

[99] S.G. Kandalkar, C.D. Lokhande, R.S. Mane, S.H. Han, A non-thermal chemical synthesis of hydrophilic and amorphous cobalt oxide films for supercapacitor application, Appl. Surf. Sci. 253 (2007) 3952–3956. doi:10.1016/j.apsusc.2006.08.026.

[100] S.G. Kandalkar, J.L. Gunjakar, C.D. Lokhande, Preparation of cobalt oxide thin films and its use in supercapacitor application, Appl. Surf. Sci. 254 (2008) 5540–5544. doi:10.1016/j.apsusc.2008.02.163.

[101] J. Lang, X. Yan, Q. Xue, Facile preparation and electrochemical characterization of cobalt oxide/multi-walled carbon nanotube composites for supercapacitors, J. Power Sources. 196 (2011) 7841–7846. doi:10.1016/j.jpowsour.2011.04.010.

[102] J. Yan, T. Wei, W. Qiao, B. Shao, Q. Zhao, L. Zhang, Z. Fan, Rapid microwave-assisted synthesis of graphene nanosheet/Co_3O_4 composite for supercapacitors, Electrochim. Acta. 55 (2010) 6973–6978. doi:10.1016/j.electacta.2010.06.081.

[103] C. Niu, J. Meng, X. Wang, C. Han, M. Yan, K. Zhao, X. Xu, W. Ren, Y. Zhao, L. Xu, Q. Zhang, D. Zhao, L. Mai, General synthesis of complex nanotubes by gradient electrospinning and controlled pyrolysis, Nat. Commun. 6 (2015) 1–9. doi:10.1038/ncomms8402.

[104] X.Y. Liu, Y.Q. Gao, G.W. Yang, A flexible, transparent and super-long-life supercapacitor based on ultrafine Co_3O_4 nanocrystal electrodes, Nanoscale. 8 (2016) 4227–4235. doi:10.1039/c5nr09145d.

[105] C. Feng, J. Zhang, Y. Deng, C. Zhong, L. Liu, W. Hu, One-pot fabrication of Co_3O_4 microspheres via hydrothermal method at low temperature for high capacity supercapacitor, Mater. Sci. Eng. B. 199 (2015) 15–21. doi:10.1016/j.mseb.2015.04.010.

[106] J. Ma, W. Zhang, L. Zheng, Y. Sun, R. Jin, G. Zhao, Y. Liu, Direct formation of (Co, Mn)$_3O_4$ nanowires/Ni composite foam for electrochemical detection, J. Alloys Compd. 663 (2016) 230–234. doi:10.1016/j.jallcom.2015.12.123.

[107] Z. Hai, L. Gao, Q. Zhang, H. Xu, D. Cui, Z. Zhang, D. Tsoukalas, J. Tang, S. Yan, C. Xue, Facile synthesis of core-shell structured PANI-Co_3O_4 nanocomposites with superior electrochemical performance in supercapacitors, Appl. Surf. Sci. 361 (2016) 57–62. doi:10.1016/j.apsusc.2015.11.171.

[108] A.N. Naveen, P. Manimaran, S. Selladurai, Cobalt oxide (Co_3O_4)/graphene nanosheets (GNS) composite prepared by novel route for supercapacitor application, J. Mater. Sci. Mater. Electron. 26 (2015) 8988–9000. doi:10.1007/s10854-015-3582-2.

[109] M. Li, J.P. Cheng, F. Liu, X.B. Zhang, In situ growth of nickel-cobalt oxyhydroxide/oxide on carbon nanotubes for high performance supercapacitors, Electrochim. Acta. 178 (2015) 439–446. doi:10.1016/j.electacta.2015.08.041.

[110] Y. Wang, H. Wang, X. Wang, The cobalt oxide/hydroxide nanowall array film prepared by pulsed laser deposition for supercapacitors with superb-rate capability, Electrochim. Acta. 92 (2013) 298–303. doi:10.1016/j.electacta.2013.01.061.

[111] C.Y. Lee, K. Lee, P. Schmuki, Anodic formation of self-organized cobalt oxide nanoporous layers, Angew. Chemie - Int. Ed. 52 (2013) 2077–2081. doi:10.1002/anie.201208793.

[112] H.E. Unalan, G. Fanchini, A. Kanwal, A. Du Pasquier, M. Chhowalla, Design criteria for transparent single-wall carbon nanotube thin-film transistors, Nano Lett. 6 (2006) 677–682. doi:10.1021/nl052406l.

[113] R. Yuksel, C. Durucan, H.E. Unalan, Ternary nanocomposite SWNT/WO_3/PANI thin film electrodes for supercapacitors, J. Alloys Compd. 658 (2016) 183–189. doi:10.1016/j.jallcom.2015.10.216.

[114] B.B. Parekh, G. Fanchini, G. Eda, M. Chhowalla, Improved conductivity of transparent single-wall carbon nanotube thin films via stable postdeposition functionalization, Appl. Phys. Lett. 90 (2007) 1–4. doi:10.1063/1.2715027.

[115] M.B. Durukan, R. Yuksel, H.E. Unalan, Cobalt oxide nanoflakes on single walled carbon nanotube thin films for supercapacitor electrodes, Electrochim. Acta. 222 (2016) 1475–1482. doi:10.1016/j.electacta.2016.11.126.

[116] Z.P. Xu, H.C. Zeng, Thermal evolution of cobalt hydroxides: a comparative study of their various structural phases, J. Mater. Chem. 8 (1998) 2499–2506. doi:10.1039/a804767g.

[117] M. Nakamura, M. Nakanishi, K. Yamamoto, Influence of physical properties of activated carbons on characteristics of electric double-layer capacitors, J. Power Sources. 60 (1996) 225–231. doi:10.1016/S0378-7753(96)80015-2.

[118] J.-C. Dupin, D. Gonbeau, P. Vinatier, A. Levasseur, Systematic XPS studies of metal oxides, hydroxides and peroxides, Phys. Chem. Chem. Phys. 2 (2000) 1319–1324. doi:10.1039/a908800h.

[119] D. Gu, C. Jia, C. Weidenthaler, H. Bongard, B. Spliethoff, W. Schmidt, F. Schüth, Highly ordered mesoporous cobalt-containing oxides: structure, catalytic properties, and active sites in oxidation of carbon monoxide, J. Am. Chem. Soc. 137 (2015) 11407–18. doi:10.1021/jacs.5b06336.

[120] C.W. Tang, C. Bin Wang, S.H. Chien, Characterization of cobalt oxides studied by FT-IR, Raman, TPR and TG-MS, Thermochim. Acta. 473 (2008) 68–73. doi:10.1016/j.tca.2008.04.015.

[121] P. Azaïs, L. Duclaux, P. Florian, D. Massiot, M.A. Lillo-Rodenas, A. Linares-Solano, J.P. Peres, C. Jehoulet, F. Béguin, Causes of supercapacitors ageing in organic electrolyte, J. Power Sources. 171 (2007) 1046–1053. doi:10.1016/j.jpowsour.2007.07.001.

[122] Y.G. Majid Beidaghi, Capacitive energy storage in micro-scale devices: recent advances in design and fabrication of micro- supercapacitors, Energy Environ. Sci. 7 (2014) 867–884. doi:10.1039/c3ee43526a.

[123] J.H. Lim, D.J. Choi, H.-K. Kim, W. Il Cho, Y.S. Yoon, Thin Film Supercapacitors Using a Sputtered RuO_2 Electrode, J. Electrochem. Soc. 148 (2001) A275. doi:10.1149/1.1350666.

[124] Y. Honda, T. Haramoto, M. Takeshige, H. Shiozaki, T. Kitamura, K. Yoshikawa, M. Ishikawa, Performance of electric double-layer capacitor with vertically aligned MWCNT sheet electrodes prepared by transfer methodology, J. Electrochem. Soc. 155 (2008) A930. doi:10.1149/1.2988743.

[125] L.T. Le, M.H. Ervin, H. Qiu, B.E. Fuchs, W.Y. Lee, Graphene supercapacitor electrodes fabricated by inkjet printing and thermal reduction of graphene oxide, Electrochem. Commun. 13 (2011) 355–358. doi:10.1016/j.elecom.2011.01.023.

[126] K. Sheng, Y. Sun, C. Li, W. Yuan, G. Shi, Ultrahigh-rate supercapacitors based on eletrochemically reduced graphene oxide for ac line-filtering., Sci. Rep. 2 (2012) 247. doi:10.1038/srep00247.

[127] M.F. El-Kady, R.B. Kaner, Scalable fabrication of high-power graphene micro-supercapacitors for flexible and on-chip energy storage., Nat. Commun. 4 (2013) 1475. doi:10.1038/ncomms2446.

[128] W. Gao, N. Singh, L. Song, Z. Liu, A.L.M. Reddy, L. Ci, R. Vajtai, Q. Zhang, B. Wei, P.M. Ajayan, Direct laser writing of micro-supercapacitors on hydrated graphite oxide films., Nat. Nanotechnol. 6 (2011) 496–500. doi:10.1038/nnano.2011.110.

[129] J. Ren, L. Li, C. Chen, X. Chen, Z. Cai, L. Qiu, Y. Wang, X. Zhu, H. Peng, Twisting carbon nanotube fibers for both wire-shaped micro-supercapacitor and micro-battery, Adv. Mater. 25 (2013) 1155–1159. doi:10.1002/adma.201203445.

[130] K. Wang, W. Zou, B. Quan, A. Yu, H. Wu, P. Jiang, Z. Wei, An all-solid-state flexible micro-supercapacitor on a chip, Adv. Energy Mater. 1 (2011) 1068–1072. doi:10.1002/aenm.201100488.

[131] C.C. Liu, D.S. Tsai, W.H. Chung, K.W. Li, K.Y. Lee, Y.S. Huang, Electrochemical micro-capacitors of patterned electrodes loaded with manganese oxide and carbon nanotubes, J. Power Sources. 196 (2011) 5761–5768. doi:10.1016/j.jpowsour.2011.02.050.

[132] C.H. Chen, D.S. Tsai, W.H. Chung, K.Y. Lee, Y.M. Chen, Y.S. Huang, Electrochemical capacitors of miniature size with patterned carbon nanotubes and cobalt hydroxide, J. Power Sources. 205 (2012) 510–515. doi:10.1016/j.jpowsour.2012.01.072.

[133] D. Pech, M. Brunet, P.L. Taberna, P. Simon, N. Fabre, F. Mesnilgrente, V. Conédéra, H. Durou, Elaboration of a microstructured inkjet-printed carbon electrochemical capacitor, J. Power Sources. 195 (2010) 1266–1269. doi:10.1016/j.jpowsour.2009.08.085.

[134] M.F. El-Kady, V. Strong, S. Dubin, R.B. Kaner, Laser Scribing of High-Performance and Flexible Graphene-Based Electrochemical Capacitors, Science 335 (2012) 1326–1330. doi:10.1126/science.1216744.

[135] C. Shen, C.-P. Wang, M. Sanghadasa, L. Lin, Flexible micro-supercapacitors prepared using direct-write nanofibers, RSC Adv. 7 (2017) 11724–11731. doi:10.1039/C6RA28218K.

[136] M. Beidaghi, C. Wang, Micro-supercapacitors based on interdigital electrodes of reduced graphene oxide and carbon nanotube composites with ultrahigh power handling performance, Adv. Funct. Mater. 22 (2012) 4501–4510. doi:10.1002/adfm.201201292.

[137] Q. Meng, H. Wu, Y. Meng, K. Xie, Z. Wei, Z. Guo, High-performance all-carbon yarn micro-supercapacitor for an integrated energy system, Adv. Mater. 26 (2014) 4100–4106. doi:10.1002/adma.201400399.

[138] J.W. Long, B. Dunn, D.R. Rolison, H.S. White, Three-dimensional battery architectures, Chem. Rev. 104 (2004) 4463–4492. doi:10.1021/cr020740l.

[139] M. Beidaghi, W. Chen, C. Wang, Electrochemically activated carbon micro-electrode arrays for electrochemical micro-capacitors, J. Power Sources. 196 (2011) 2403–2409. doi:10.1016/j.jpowsour.2010.09.050.

[140] C. Shen, X. Wang, W. Zhang, F. Kang, A high-performance three-dimensional micro supercapacitor based on self-supporting composite materials, J. Power Sources. 196 (2011) 10465–10471. doi:10.1016/j.jpowsour.2011.08.007.

[141] W. Chen, M. Beidaghi, V. Penmatsa, K. Bechtold, L. Kumari, W.Z. Li, C. Wang, Integration of carbon nanotubes to C-MEMS for on-chip supercapacitors, IEEE Trans. Nanotechnol. 9 (2010) 734–740. doi:10.1109/TNANO.2010.2049500.

[142] W. Sun, R. Zheng, X. Chen, Symmetric redox supercapacitor based on micro-fabrication with three-dimensional polypyrrole electrodes, J. Power Sources. 195 (2010) 7120–7125. doi:10.1016/j.jpowsour.2010.05.012.

[143] M. Beidaghi, C. Wang, Micro-supercapacitors based on three dimensional interdigital polypyrrole/C-MEMS electrodes, Electrochim. Acta. 56 (2011) 9508–9514. doi:10.1016/j.electacta.2011.08.054.

[144] Y. Gogotsi, P. Simon, True performance metrics in electrochemical energy storage, 189 (2012) 917–918. doi:10.1126/science.1213003.

[145] T.S. Arthur, D.J. Bates, N. Cirigliano, D.C. Johnson, P. Malati, J.M. Mosby, E. Perre, M.T. Rawls, A.L. Prieto, B. Dunn, Three-dimensional electrodes and battery architectures, MRS Bull. 36 (2011) 523–531. doi:10.1557/mrs.2011.156.

[146] D. Pech, M. Brunet, H. Durou, P. Huang, V. Mochalin, Y. Gogotsi, P. Taberna, P. Simon, Ultrahigh-power micrometre-sized supercapacitors based on onion-like carbon, Nat. Nanotechnol. 5 (2010) 651–654. doi:10.1038/nnano.2010.162.

[147] W. Gao, N. Singh, L. Song, Z. Liu, A.L.M. Reddy, L. Ci, R. Vajtai, Q. Zhang, B. Wei, P.M. Ajayan, Direct laser writing of micro-supercapacitors on hydrated graphite oxide films., Nat. Nanotechnol. 6 (2011) 496–500. doi:10.1038/nnano.2011.110.